Studies of the decay Ds+→K+K−μ+νμ

BESIII Collaboration; Kalantar-Nayestanaki, N.; Kappert, R.; Kavatsyuk, M.; Messchendorp, J.; Rodin, V.

Published in:
Journal of High Energy Physics

DOI:
10.1007/JHEP12(2023)072

Publication date:
2023

Published for SISSA by Springer

Received: *July 19, 2023*
Accepted: *November 23, 2023*
Published: *December 12, 2023*

Studies of the decay $D_s^+ \to K^+K^-\mu^+\nu_\mu$

The BESIII collaboration

E-mail: besiii-publications@ihep.ac.cn

Abstract: The $D_s^+ \to K^+K^-\mu^+\nu_\mu$ decay is studied based on 7.33 fb^{-1} of e^+e^- collision data collected with the BESIII detector at center-of-mass energies in the range from 4.128 to 4.226 GeV. The absolute branching fraction is measured as $\mathcal{B}(D_s^+ \to \phi\mu^+\nu_\mu) = (2.25 \pm 0.09 \pm 0.07) \times 10^{-2}$, the most precise measurement to date. Combining with the world average of $\mathcal{B}(D_s^+ \to \phi e^+\nu_e)$, the ratio of the branching fractions obtained is $\frac{\mathcal{B}(D_s^+\to\phi\mu^+\nu_\mu)}{\mathcal{B}(D_s^+\to\phi e^+\nu_e)} = 0.94 \pm 0.08$, in agreement with lepton universality. By performing a partial wave analysis, the hadronic form factor ratios at $q^2 = 0$ are extracted, finding $r_V = \frac{V(0)}{A_1(0)} = 1.58 \pm 0.17 \pm 0.02$ and $r_2 = \frac{A_2(0)}{A_1(0)} = 0.71 \pm 0.14 \pm 0.02$, where the first uncertainties are statistical and the second are systematic. No significant S-wave contribution from $f_0(980) \to K^+K^-$ is found. The upper limit $\mathcal{B}(D_s^+ \to f_0(980)\mu^+\nu_\mu) \cdot \mathcal{B}(f_0(980) \to K^+K^-) < 5.45 \times 10^{-4}$ is set at 90% credibility level.

Keywords: Branching fraction, Charm Physics, e^+-e^- Experiments

ArXiv ePrint: 2307.03024

https://doi.org/10.1007/JHEP12(2023)072

JHEP12(2023)072

Contents

JHEP12(2023)072

1 Introduction

The study of charm semileptonic (SL) decays provides valuable information about weak and strong interactions in mesons composed of heavy quarks. The SL partial decay width is related to the product of the hadronic form factors (FFs) describing the strong interactions between final-state quarks, including non-perturbative effects, and the Cabibbo-Kobayashi-Maskawa (CKM) matrix elements. Precise measurements of FFs are important for comparison with the theoretical calculations. From the theoretical point of view, hadronic FFs play a crucial role in the study of leptonic D_s decays. They are calculated by non-perturbative methods, including lattice quantum chromodynamics (LQCD) [1–4] and phenomenological quark models. The latter category includes the covariant confined quark model (CCQM) [5], the constituent quark model (CQM) [6], the light-front quark model (LFQM) [7], as well as the HMχT model [8] (based on the combination of heavy meson and chiral symmetries). The $D_s^+ \to \phi\ell^+\nu_\ell$ decay is particularly interesting since the ϕ meson is a narrow resonance, which can be isolated, providing a good testbed.

In the Standard Model (SM), SL decays offer an excellent opportunity to test lepton flavor universality (LFU) and search for new physics effects. Previously, LHCb tests of LFU using $B^+ \to K^+\ell^+\ell^-$ decays hinted at LFU violation, with a significance of 3.1σ [9]. However, more recently LHCb tests of LFU in $B^+ \to K^+\ell^+\ell^-$ and $B^0 \to K^{*0}\ell^+\ell^-$ decays [10] are consistent with the SM at the 1.0σ level. The possible tension is addressed by various theoretical models [11–15]. Searches for LFU violation have also been performed in SL decays of $D^{0(+)}$ and D_s^+ mesons [16–21] and baryons [22–25], without any clear evidence for deviation with respect to the SM predictions. Hence, higher precision measurements are desirable. For $D_s^+ \to \phi\ell^+\nu_\ell$ decays, *BABAR* performed the most precise measurement of the absolute branching fraction (BF) of $D_s^+ \to \phi e^+\nu_e$ with an uncertainty of 6.6% [26]. In comparison, the uncertainty of the BF of $D_s^+ \to \phi\mu^+\nu_\mu$ measured by the BESIII experiment previously is 26.3% [20], which limits the precision of LFU studies using $D_s^+ \to \phi\ell^+\nu_\ell$ decays. Therefore, a precision measurement of the absolute BF of $D_s^+ \to \phi\mu^+\nu_\mu$ can provide a critical, complementary test for LFU.

Using the $7.33\,\text{fb}^{-1}$ data sample collected by BESIII at center-of-mass energies (E_{CM}) in the range from 4.128 to 4.226 GeV, a measurement of the BF of the $D_s^+ \to \phi\mu^+\nu_\mu$ decay with significantly improved precision is reported. LFU is tested using the world average value of the $D_s^+ \to \phi e^+\nu_e$ BF. Additionally, the hadronic FFs of $D_s^+ \to \phi\mu^+\nu_\mu$ are extracted through a partial wave analysis (PWA) and the size of a possible $f_0(980)$ component in the decay $D_s^+ \to K^+K^-\mu^+\nu_\mu$ is limited. An $f_0(980)$ contribution would be interesting, in view of the unconventional nature of this state [27–31]. Charge conjugation is implied throughout this work.

2 Detector and Monte Carlo simulations

The BESIII detector [32] records symmetric e^+e^- collisions provided by the BEPCII storage ring [33] in the E_{CM} range from 2.0 to 4.95 GeV, with a peak luminosity of $1\times10^{33}\,\text{cm}^{-2}\,\text{s}^{-1}$ achieved at $E_{\text{CM}} = 3.77$ GeV. BESIII has collected large data samples in this energy region [34, 35]. The cylindrical core of the BESIII detector covers 93% of the full solid angle and consists of a helium-based multilayer drift chamber (MDC), a plastic scintillator time-of-flight system (TOF), and a CsI(Tl) electromagnetic calorimeter (EMC), which are all enclosed in a superconducting solenoidal magnet providing a 1.0 T magnetic field [36]. The solenoid is supported by an octagonal flux-return yoke with resistive plate counter muon identification modules interleaved with steel. The charged-particle momentum resolution at 1 GeV/c is 0.5%, and the resolution of the specific ionization energy loss (dE/dx) is 6% for electrons from Bhabha scattering. The EMC measures photon energies with a resolution of 2.5% (5%) at 1 GeV in the barrel (end cap) region. The time resolution in the TOF barrel region is 68 ps. The end cap TOF system was upgraded in 2015 using multi-gap resistive plate chamber technology, providing a time resolution of 60 ps [37]. About 83% of the dataset used in this analysis benefits from this upgrade.

The data samples corresponding to a total integrated luminosity of $7.33\,\text{fb}^{-1}$ are used in this analysis. The integrated luminosity of each data sample is shown in table 1 [38, 39]. Simulated data samples produced with a GEANT4-based [40] Monte Carlo (MC) package,

JHEP12(2023)072

$E_{\rm CM}$ (GeV)	$\mathcal{L}_{\rm int}$ (pb^{-1})	$M_{\rm BC}$ (GeV/c^2)	$N_j^{\rm ST}$	$\bar{\epsilon}_j$ (%)
4.128	401.5	[2.010, 2.061]	31803 ± 695	18.07 ± 0.06
4.157	408.7	[2.010, 2.070]	51026 ± 839	19.03 ± 0.06
4.178	$3189.0 \pm 0.2 \pm 31.9$	[2.010, 2.073]	401179 ± 2487	18.84 ± 0.05
4.189	$570.0 \pm 0.1 \pm 2.2$	[2.010, 2.076]	67575 ± 927	19.97 ± 0.06
4.199	$526.0 \pm 0.1 \pm 2.1$	[2.010, 2.079]	63076 ± 950	19.51 ± 0.06
4.209	$572.1 \pm 0.1 \pm 1.8$	[2.010, 2.082]	63119 ± 1052	20.24 ± 0.06
4.219	$569.2 \pm 0.1 \pm 1.8$	[2.010, 2.085]	53466 ± 943	20.46 ± 0.06
4.226	$1100.9 \pm 0.1 \pm 7.0$	[2.010, 2.088]	85390 ± 1551	21.64 ± 0.06

Table 1. The integrated luminosities ($\mathcal{L}_{\rm int}$), the requirements on $M_{\rm BC}$, the total ST yields ($N_j^{\rm ST}$), and the averaged signal efficiencies ($\bar{\epsilon}_j = (\sum_\alpha (N_{\alpha,j}^{\rm ST}/N_j^{\rm ST}) \cdot (\epsilon_{\alpha,{\rm sig},j}^{\rm DT}/\epsilon_{\alpha,j}^{\rm ST}))$) at various energy points. The first and second uncertainties are statistical and systematic, respectively. The $\mathcal{L}_{\rm int}$ for data samples of $E_{\rm CM} = 4.128\,{\rm GeV}$ and $E_{\rm CM} = 4.157\,{\rm GeV}$ are estimated by using online monitoring information. The definition of $M_{\rm BC}$ is given in eq. (4.1). The efficiencies do not include the BF of $\phi \to K^+K^-$.

which includes the geometric description of the BESIII detector and the detector response, are used to determine detection efficiencies and to estimate backgrounds. The simulation models the beam energy spread and initial state radiation (ISR) in the e^+e^- annihilations with the generator KKMC [41]. An inclusive MC sample with a luminosity equivalent to 40 times that of data is generated at $E_{\rm CM} \in [4.128, 4.226]$ GeV. This MC is used to determine the distributions of kinematic variables and estimate the detection efficiency. It includes the production of open charm processes, the ISR production of vector charmonium(-like) states, and the continuum processes incorporated in KKMC [41]. The production of open charm states directly via e^+e^- annihilations is modeled with the generator CONEXC [42], and their subsequent decays are modeled by EVTGEN [43, 44] with known BFs from the Particle Data Group (PDG) [45]. The ISR production of vector charmonium(-like) states and the continuum processes are incorporated in KKMC [41]. The remaining unknown charmonium decays are modelled with LUNDCHARM [46, 47]. Final state radiation (FSR) from charged final-state particles is incorporated using the PHOTOS package [48]. A phase-space (PHSP) MC sample is produced for $D_s^+ \to K^+K^-\mu^+\nu_\mu$ and is used to extract the detection efficiency. Initially, this PHSP MC sample is used to calculate the normalization integral used in the determination of the amplitude model parameters in the fit to data. Then, the signal MC sample is regenerated with the D_s^+ meson decaying to $K^+K^-\mu^+\nu_\mu$ using the fitted amplitude model. It is used to find the final PWA solution and obtain the signal efficiency.

3 Analysis method

A double-tag (DT) method is used in this analysis following refs. [49–51]. At $E_{\rm CM}$ between 4.128 and 4.226 GeV, D_s mesons are mainly produced via the process $e^+e^- \to D_s^{*+}[\to$

JHEP12(2023)072

$\gamma(\pi^0)D_s^+]D_s^-$. One D_s^- meson is fully reconstructed in one of the hadronic decay modes, called a single-tag (ST) candidate. Based on this, among the particles recoiling against the ST D_s^- meson, we select the signal decay of the D_s^+ meson and a transition $\gamma(\pi^0)$ from the D_s^{*+}; success results in a double-tag (DT) candidate.

To measure the BF of the signal decay, the following equations for one ST mode are used:

$$N_{\rm tag}^{\rm ST} = 2N_{D_s^{*\pm}D_s^{\mp}}\mathcal{B}_{\rm tag}\epsilon_{\rm tag}^{\rm ST}\,, \tag{3.1}$$

$$N_{\rm tag,sig}^{\rm DT} = 2N_{D_s^{*\pm}D_s^{\mp}}\mathcal{B}_{\rm tag}\mathcal{B}_{\rm sig}\epsilon_{\rm tag,sig}^{\rm DT}\,, \tag{3.2}$$

where $N_{\rm tag}^{\rm ST}$ is the ST yield for the tag mode, $N_{\rm tag,sig}^{\rm DT}$ is the DT yield, $N_{D_s^{*\pm}D_s^{\mp}}$ is the total number of $D_s^{*\pm}D_s^{\mp}$ pairs produced in the e^+e^- collisions, $\mathcal{B}_{\rm tag}$ and $\mathcal{B}_{\rm sig}$ are the BFs of the tag and signal modes, respectively, $\epsilon_{\rm tag}^{\rm ST}$ is the ST efficiency to reconstruct the tag mode and $\epsilon_{\rm tag,sig}^{\rm DT}$ is the DT efficiency to reconstruct both the tag and signal decay modes. In the case of more than one tag mode and energy point, eq. (3.2) can be written as

$$N_{\rm total}^{\rm DT} = \sum_{\alpha,j} N_{\alpha,{\rm sig},j}^{\rm DT} = \mathcal{B}_{\rm sig}\sum_{\alpha,j} 2N_{D_s^{*\pm}D_s^{\mp}}^{j}\mathcal{B}_{\alpha}\epsilon_{\alpha,{\rm sig},j}^{\rm DT}\,, \tag{3.3}$$

where α represents the tag-mode and j is the energy point (from 0 to 7, corresponding to the energy points in table 1). $\mathcal{B}_{\rm sig}$ is isolated by using eq. (3.1):

$$\mathcal{B}_{\rm sig} = \frac{N_{\rm total}^{\rm DT}}{\sum\limits_{\alpha,j} N_{\alpha,j}^{\rm ST}\epsilon_{\alpha,{\rm sig},j}^{\rm DT}/\epsilon_{\alpha,j}^{\rm ST}\cdot\mathcal{B}_{\rm sub}}, \tag{3.4}$$

where $N_{\rm total}^{\rm DT}$ denotes the total number of DT events obtained from the fit to the signal peaks (see below) of the selected DT candidates, while $N_{\alpha,j}^{\rm ST}$ and $\epsilon_{\alpha,j}^{\rm ST}$ are obtained from the data and inclusive MC samples, respectively. Finally, $\epsilon_{\alpha,{\rm sig},j}^{\rm DT}$ is determined with signal MC samples. These efficiencies do not include the product of the BFs, $\mathcal{B}_{\rm sub}$, for the intermediate resonance decays.

4 Single tag selection

Candidates for the ST D_s^- mesons are reconstructed via fourteen hadronic decay modes $D_s^- \to K^+K^-\pi^-$, $K^-\pi^+\pi^-$, $\pi^+\pi^-\pi^-$, $K^+K^-\pi^-\pi^0$, $\eta'_{\gamma\rho^0}\pi^-$, $\eta_{\gamma\gamma}\rho^-$, $K_S^0K^-\pi^+\pi^-$, $K_S^0K^+\pi^-\pi^-$, $\eta_{\gamma\gamma}\pi^-$, $K_S^0K_S^0\pi^-$, $\eta_{\pi^0\pi^+\pi^-}\pi^-$, $\eta'_{\eta_{\gamma\gamma}\pi^+\pi^-}\pi^-$, $K_S^0K^-\pi^0$, and $K_S^0K^-$. Throughout this paper, the subscripts of η and η' indicate the decay modes used for reconstructing the corresponding particle.

The selection criteria of $\pi^\pm$, $K^\pm$, K_S^0, γ, π^0, and η candidates follow refs. [19, 52]. All charged tracks are required to be within $|\cos\theta| < 0.93$, where θ is the polar angle defined with respect to the symmetry axis of the MDC. For the charged tracks that are not from K_S^0 decays, the distance of closest approach to the interaction point must be less than 10 cm along the beam direction and less than 1 cm in the plane perpendicular to the beam. Particle identification (PID) of the charged particles is performed by combining $\mathrm{d}E/\mathrm{d}x$ measurements in the MDC with flight time measurements in the TOF system. Tracks are

JHEP12(2023)072

identified by the PID likelihood $\mathcal{L}_h$ ($h = \pi, K$) for each hadron h hypothesis. Pion and kaon candidates are required to satisfy $\mathcal{L}_\pi > \mathcal{L}_K$ and $\mathcal{L}_K > \mathcal{L}_\pi$, respectively.

The K_S^0 candidates are selected by looping over all pairs of tracks with opposite charges, which distances to the interaction point along the beam direction are within 20 cm; these tracks are treated as pions without applying PID. The $\pi^+\pi^-$ invariant mass is required to be in the range of $(0.487, 0.511)$ GeV/c^2. The signed decay length, L, of the reconstructed K_S^0 is required to be separated from the interaction point by greater than twice its resolution, σ: $L/\sigma > 2$.

Photon shower candidates are selected from energy clusters in the EMC that are not associated with any charged track. To reduce the number of photon candidates that result from noise and beam background, each shower is required to start within 700 ns of the event start time. The deposited energy of showers in the barrel region and in the end-cap region must be greater than 25 MeV and 50 MeV [32], respectively. To exclude showers that originate from charged tracks, the angle subtended by the EMC shower and the position of the closest charged track at the EMC must be greater than 10 degrees as measured from the interaction point.

Photon pairs are used to reconstruct the π^0 and η mesons. The invariant masses of the selected photon pairs are required to be within the intervals $(0.115, 0.150)$ and $(0.500, 0.570)$ GeV/c^2, respectively. To improve the momentum resolution and suppress background contributions, a kinematic fit is applied to each selected photon pair, whose invariant mass is constrained to the nominal mass of π^0 or η [45].

For the $D_s^- \to \eta_{\pi^0\pi^+\pi^-}\pi^-$ tag mode, the invariant mass $M_{\pi^0\pi^+\pi^-}$ of the $\pi^0\pi^+\pi^-$ combinations used to form η candidates is required to be within the interval $(0.530, 0.570)$ GeV/c^2. The two decay modes $\eta\pi^+\pi^-$ and $\gamma\rho^0$ are used to reconstruct η' candidates, while their invariant masses are required to fall in the ranges of $(0.946, 0.970)$ GeV/c^2 and $(0.940, 0.976)$ GeV/c^2, respectively. Additionally, the energy of the γ from $\eta' \to \gamma\rho^0$ decays are required to be greater than 0.1 GeV. The $\pi^+\pi^-$ and $\pi^-\pi^0$ combinations are used to form ρ^0 and ρ^- candidates, respectively, and their invariant masses are required to fall in the range of $(0.570, 0.970)$ GeV/c^2.

To suppress the transition pions from $D^{*+} \to D^0\pi^+$, the minimum momenta of all the pions, which are not from the K_S^0, η, or η' decays, must be greater than 0.1 GeV/c. For the $D_s^- \to K^-\pi^+\pi^-$ and $D_s^- \to \pi^+\pi^-\pi^-$ tag modes, the peaking background events from $D_s^- \to K_S^0K^-$ and $D_s^- \to K_S^0\pi^-$ are suppressed by requiring the $\pi^+\pi^-$ invariant mass to be at least 0.03 GeV/c^2 away from the known K_S^0 mass [45].

To reject the non-$D_s^\pm D_s^{*\mp}$ backgrounds, we define the beam-constrained mass of the ST D_s^- candidate as

$$M_{\rm BC} \equiv \sqrt{E_{\rm CM}^2/4 - |\vec{p}_{D_s^-}|^2} \tag{4.1}$$

and require $M_{\rm BC}$ to be within the region listed in table 1. This selection criterion accepts most of the D_s^- mesons from the $e^+e^- \to D_s^\pm D_s^{*\mp}$ process.

If there are multiple combinations in one event, only the candidate with the D_s^- recoil mass

$$M_{\rm rec} \equiv \sqrt{\left(E_{\rm CM} - \sqrt{|\vec{p}_{D_s^-}|^2 + m_{D_s^-}^2}\right)^2 - |\vec{p}_{D_s^-}|^2} \tag{4.2}$$

JHEP12(2023)072

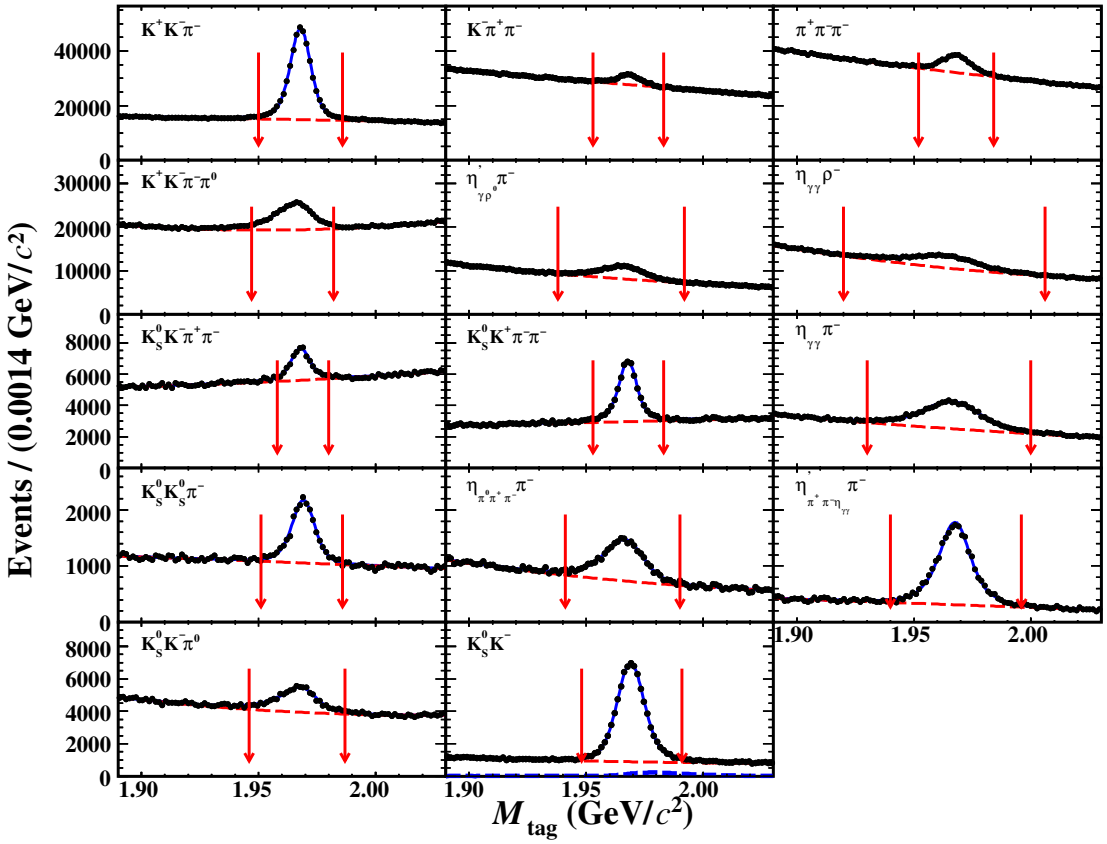

Figure 1. Fits to the $M_{\rm tag}$ distributions of the ST D_s^- candidates. Points with error bars are data for all energy points. Blue solid lines are the best fits. Red dashed lines are the fitted background shapes. For the $K_S^0K^-$ tag mode, the blue doted line is from the $D^- \to K_S^0\pi^-$ background. For each tag mode, the $M_{\rm tag}$ signal region are denoted by the pair of red arrows.

closest to the D_s^{*+} nominal mass [45] is kept for further analysis per tag mode per charge. Here, $\vec{p}_{D_s^-}$ is the momentum of the D_s^- candidate and $m_{D_s^-}$ is the nominal D_s^- meson [45]. Figure 1 shows the invariant mass ($M_{\rm tag}$) spectra of the accepted ST D_s^- candidates for the individual tag modes in data combined from all energy points. The ST yield for each tag mode is obtained through fitting the corresponding $M_{\rm tag}$ spectrum. In the fit, the signal is modeled by the simulated shape, for events where the solid angle between the generated and reconstructed four-momentum is no more than 15°, convolved with a Gaussian function to take into account the resolution difference between data and simulation.

For the $D_s^- \to K_S^0K^-$ tag mode, there is a peaking background from $D^- \to K_S^0\pi^-$, which is modeled by the simulated shape convolved with the same Gaussian function used in the signal shape with its size left as a free parameter. A second-order polynomial is used to describe the non-peaking background, which has been validated with the inclusive MC sample. The fit results are shown in figure 1. Events within the signal regions are kept for the further analyses. As an example, the ST yields ($N^{\rm ST}_{\alpha,2}$) for different tag modes in data at $E_{\rm CM} = 4.178\,{\rm GeV}$ and the corresponding ST and DT efficiencies ($\epsilon^{\rm ST}_{\alpha,2}, \epsilon^{\rm DT}_{\alpha,{\rm sig},2}$) are summarized in table 2. The values of $N^{\rm ST}_{\alpha,j}$ and $\epsilon^{\rm ST}_{\alpha,j}$ at the other energy points are obtained similarly. The ST yields $N^{\rm ST}_j$ in data and the averaged signal efficiencies $\bar{\epsilon}_j$ at each energy

JHEP12(2023)072

Tag mode	$N^{\rm ST}_{\alpha,2}$	$\epsilon^{\rm ST}_{\alpha,2}$ (%)	$\epsilon^{\rm DT}_{\alpha,{\rm sig},2}$ (%)
$K^+K^-\pi^-$	137317 ± 608	40.92 ± 0.02	6.84 ± 0.03
$K^-\pi^+\pi^-$	16514 ± 632	45.42 ± 0.07	8.52 ± 0.12
$\pi^+\pi^-\pi^-$	36497 ± 873	52.13 ± 0.05	9.97 ± 0.09
$K^+K^-\pi^-\pi^0$	42119 ± 851	11.77 ± 0.01	2.03 ± 0.02
$\eta'_{\gamma\rho^0}\pi^-$	24698 ± 656	32.53 ± 0.04	6.78 ± 0.08
$\eta_{\gamma\gamma}\rho^-$	39670 ± 1673	19.88 ± 0.02	4.99 ± 0.04
$K^0_SK^-\pi^+\pi^-$	7621 ± 270	18.51 ± 0.05	3.07 ± 0.07
$K^0_SK^+\pi^-\pi^-$	14855 ± 235	21.12 ± 0.04	3.68 ± 0.06
$\eta_{\gamma\gamma}\pi^-$	19239 ± 468	48.79 ± 0.06	9.97 ± 0.12
$K^0_SK^0_S\pi^-$	5088 ± 149	22.82 ± 0.07	4.20 ± 0.10
$\eta_{\pi^+\pi^-\pi^0}\pi^-$	5693 ± 201	23.49 ± 0.07	4.83 ± 0.11
$\eta'_{\pi^+\pi^-\eta_{\gamma\gamma}}\pi^-$	9730 ± 140	25.26 ± 0.05	4.89 ± 0.08
$K^0_SK^-\pi^0$	11182 ± 449	17.01 ± 0.04	3.64 ± 0.06
$K^0_SK^-$	30956 ± 261	47.63 ± 0.05	9.29 ± 0.09

Table 2. The obtained values of $N^{\rm ST}_{\alpha,2}$, $\epsilon^{\rm ST}_{\alpha,2}$, and $\epsilon^{\rm DT}_{\alpha,{\rm sig},2}$ in the α tag mode at $E_{\rm CM}=4.178\,{\rm GeV}$, where the efficiencies do not include the BFs for the intermediate resonance decays and the uncertainties are statistical only.

point are summarized in table 1. Summing over all tag modes and energy points gives the total ST yield to be $N^{\rm tot}_{\rm ST}=816634\pm3679$, where the uncertainty is statistical only.

5 Selection of $D_s^+\to K^+K^-\mu^+\nu_\mu$

After the selection of the tagged D_s^- candidate, a transition γ or π^0 is searched for among the unused (by the ST) photon candidates passing the basic criteria mentioned before. All possible γ or π^0 candidates are looped over; if there are multiple candidates, the one giving the minimum $|\Delta E|$ is kept. Here, $|\Delta E|$ is defined as

$$\Delta E\equiv E_{\rm CM}-E_{D_s^-}-\sqrt{|-\vec{p}_{\gamma(\pi^0)}-\vec{p}_{D_s^-}|^2+m^2_{D_s^+}}-E_{\gamma(\pi^0)}, \tag{5.1}$$

with E_{γ,π^0,D_s^-} and $\vec{p}_{\gamma,\pi^0,D_s^-}$ being the respective energy and momentum. In the presence of the ST D_s^- and transition $\gamma(\pi^0)$, the final state particles of the signal decay are selected from among the residual tracks. K^+ and K^- candidates are selected in a similar manner as the ST decay products. The muon candidates are identified based on combined information of the ${\rm d}E/{\rm d}x$ measurement from the MDC, the TOF data and the energy deposit in the EMC. The combined likelihoods $\mathcal{L}_e$, $\mathcal{L}_\mu$, and $\mathcal{L}_K$ for the electron, muon, and kaon hypotheses are calculated and the muon candidates are required to satisfy $\mathcal{L}_\mu>\mathcal{L}_K$, $\mathcal{L}_\mu>\mathcal{L}_e$, and $\mathcal{L}_\mu>0.001$. Then, with information of the ST side, two kaons, muon, and γ (π^0), $U_{\rm miss}$ is defined as:

$$U_{\rm miss}\equiv\left(E_{\rm CM}-E_{D_s^-}-E_{\gamma/\pi^0}-E_{K^+K^-}-E_{\mu^+}\right)-\left|\vec{p}_{D_s^-}+\vec{p}_{\gamma/\pi^0}+\vec{p}_{K^+K^-}+\vec{p}_{\mu^+}\right| \tag{5.2}$$

as a signal variable related to the missing neutrino. To improve the $U_{\rm miss}$ resolution, the candidate tracks and the missing neutrino are subjected to a 3-constraint kinematic fit. Energy and momentum conservation along with three mass constraints is applied while the neutrino four-vector is determined. The invariant masses of the two D_s mesons are constrained to the nominal D_s mass. Finally, the invariant mass of the $D_s^-\gamma(\pi^0)$ or $D_s^+\gamma(\pi^0)$ combinations are constrained to the nominal D_s^* mass, and the $D_s\gamma(\pi^0)$ combination with the smaller χ^2_{3C} is kept.

It is required that both the number of unused reconstructed charged tracks ($N^{\rm char}_{\rm extra}$) and unused π^0 ($N^{\pi^0}_{\rm extra}$) candidates should be zero in all DT candidate events. To suppress the peaking background of $D_s^+ \to K^+K^-\pi^+$, which is caused by misidentifying a π^+ as a μ^+, $M_{K^+K^-\nu_\mu}$ is required to be greater than $1.30\,{\rm GeV}/c^2$. To reject the remaining background of $D_s^+ \to K^+K^-\pi^+$, it is also required that $M_{K^+K^-\mu^+}$ is less than $1.75\,{\rm GeV}/c^2$. To suppress the peaking background of $D_s^+ \to K^+K^-\pi^+\pi^0$, which is mainly caused by misidentifying a the π^+ as a μ^+ and missing the π^0, the maximal energy of the photons ($E^{\rm max}_{\gamma\,{\rm extra}}$) is required to be less than 0.2 GeV. All requirements are obtained by optimizing the figure of merit defined by $S/\sqrt{S+B}$, where S and B denote the signal and background yields based on normalized inclusive MC samples. The optimizations of all requirements have been iterated for several times to obtain stable cuts.

6 Branching fraction measurement

After imposing all of the aforementioned selection criteria, the resulting $U_{\rm miss}$ distribution of the accepted $D_s^+ \to K^+K^-\mu^+\nu_\mu$ candidate events in the data sample is shown in figure 2. To extract the signal yield, an unbinned extended maximum likelihood fit is performed on this distribution. The signal is modeled by the MC-simulated shape convolved with a Gaussian function, which represents the resolution difference between data and MC samples. The peaking background of $D_s^+ \to K^+K^-\pi^+$ is fixed according to the MC simulations and the peaking background of $D_s^+ \to K^+K^-\pi^+\pi^0$ is allowed to float. Other backgrounds are dominated by processes of open charm production and continuum $q\bar{q}$, which are modeled by the inclusive MC simulation with a luminosity about 40 times that of the data sample.

The PWA (described later) shows that the only significant resonance contribution to the K^+K^- system is $D_s^+ \to \phi\mu^+\nu_\mu$. Using eq. (3.4), where the $\mathcal{B}_{\phi\to K^+K^-} = (49.1 \pm 0.5) \times 10^{-2}$ [45] and the signal yield is 1725 ± 68, the ST yield and the ST/DT efficiencies are mentioned in section 4, the corresponding BF is determined to be $\mathcal{B}(D_s^+ \to \phi\mu^+\nu_\mu) = (2.25 \pm 0.09 \pm 0.07) \times 10^{-2}$, where the first uncertainty is statistical, while the second is systematic. The systematic uncertainties will be described in more detail in section 8.

7 Partial wave analysis

To obtain data samples with high purity for the PWA, two further constraints of $|U_{\rm miss}| < 0.02\,{\rm GeV}$ and $\chi^2_{3C} < 100$ are imposed on the accepted candidates. After these conditions, 939 signal events remain, with an estimated average background level of $(9.8 \pm 0.7)\%$ at all energy points.

JHEP12(2023)072

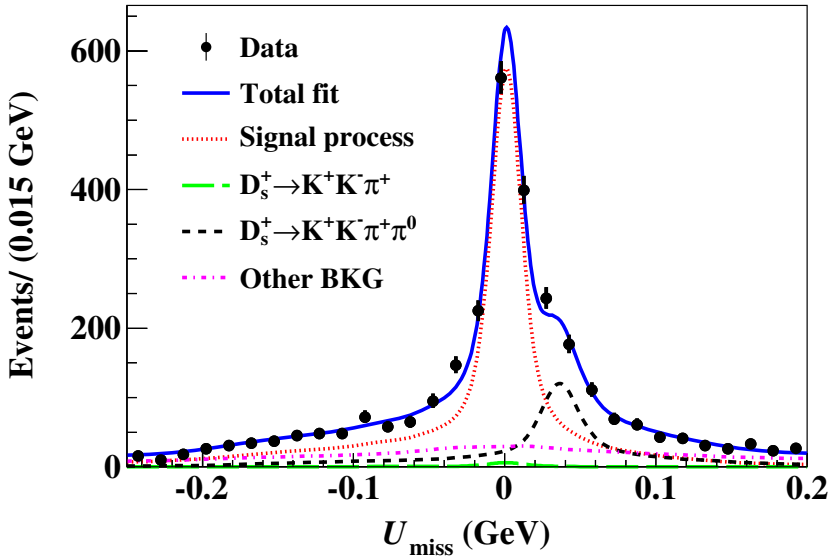

Figure 2. Fit to the $U_{\rm miss}$ distribution of the candidate events for $D_s^+ \to K^+K^-\mu^+\nu_\mu$. Points with error bars represent data. The blue solid curve denotes the total fit. The red dotted curve shows the signal process. Green long-dashed, black short-dashed, and dash-dotted violet curve are the background contributions from $D_s^+ \to K^+K^-\pi^+$, $D_s^+ \to K^+K^-\pi^+\pi^0$, and the other background contributions, respectively.

7.1 Kinematics and decay rate formalism

The differential decay rate for $D_s^+ \to K^+K^-\mu^+\nu_\mu$ depends on five variables [53]: m, the invariant mass of the K^+K^- system; q, the invariant mass of the $\mu^+\nu_\mu$ system; θ_μ (θ_K), the angle between the momentum of the μ^+ (K^-) in the $\mu^+\nu_\mu(K^+K^-)$ rest frame and the momentum of the $\mu^+\nu_\mu$ (K^+K^-) system in the D_s^+ rest frame; and χ, the angle between the normals of the decay planes defined in the D_s^+ rest frame by the K^+K^- pair and the $\mu^+\nu_\mu$ pair.

The differential decay rate as a function of these variables is given in ref. [53]. The formula is updated in ref. [54], based on chiral perturbation theory and heavy-quark symmetry; muon mass effects are treated in ref. [55]. The differential decay width of $D_s^+ \to K^+K^-\mu^+\nu_\mu$ is expressed as

$$d^5\Gamma = \frac{G_F^2|V_{cs}|^2}{(4\pi)^6 m_{D_s}^3} X\beta_m\beta_l\,\mathcal{I}(m^2, q^2, \theta_{K^-}, \theta_\mu, \chi)\, dm^2 dq^2 d\cos\theta_{K^-} d\cos\theta_\mu d\chi, \tag{7.1}$$

where $X = p_{K^+K^-} m_{D_s}$, $p_{K^+K^-}$ is the modulus of the momentum of the K^+K^- in the D_s^+ rest frame, $\beta_m = 2p^*/m$ and $\beta_l = 2p'/q$, in which p^* is the modulus of the momentum of the K^- in the K^+K^- rest frame, while p' is defined as the modulus of the momentum of μ^+ in the $\mu^+\nu_\mu$ rest frame. The Fermi coupling constant is denoted by G_F. The decay density $\mathcal{I}$ is given by

$$\begin{aligned}\mathcal{I} = {} & \mathcal{I}_1 + \mathcal{I}_2 \cos 2\theta_\mu + \mathcal{I}_3 \sin^2\theta_\mu \cos 2\chi + \mathcal{I}_4 \sin 2\theta_\mu \cos\chi + \mathcal{I}_5 \sin\theta_\mu \cos\chi \\ & + \mathcal{I}_6 \cos\theta_\mu + \mathcal{I}_7 \sin\theta_\mu \sin\chi + \mathcal{I}_8 \sin 2\theta_\mu \sin\chi + \mathcal{I}_9 \sin^2\theta_\mu \sin 2\chi,\end{aligned} \tag{7.2}$$

JHEP12(2023)072

where $\mathcal{I}_{1,\ldots,9}$ depend on m^2, q^2, and θ_{K^-}. These quantities can be expressed in terms of the four FFs $\mathcal{F}_{1,2,3,4}$. Then one can expand $\mathcal{F}_{i=1,2,3,4}$ into partial wave amplitudes including S-wave ($\mathcal{F}_{10}$), P-wave ($\mathcal{F}_{i1}$), and D-wave ($\mathcal{F}_{i2}$), to show their explicit dependence on θ_{K^-}. The detailed formulas can be found in ref. [55]. Based on the existing data, we do not find D-wave components, so the amplitude $\mathcal{F}_{i2}$ is ignored. Consequently, the FFs can be written as

$$\mathcal{F}_1 = \mathcal{F}_{10} + \mathcal{F}_{11}\cos\theta_{K^-}, \quad \mathcal{F}_2 = \frac{1}{\sqrt{2}}\mathcal{F}_{21}, \quad \mathcal{F}_3 = \frac{1}{\sqrt{2}}\mathcal{F}_{31}, \quad \mathcal{F}_4 = \mathcal{F}_{41}\cos\theta_{K^-}, \tag{7.3}$$

where $\mathcal{F}_{i1}$ can be parameterized with the helicity basis FFs $H_{0,\pm}(q^2)$. The helicity FFs can in turn be related to two axial-vector FFs $A_{1,2}(q^2)$ and one vector FF $V(q^2)$. The $A_{1,2}(q^2)$ and $V(q^2)$ all take the simple pole form $A_i(q^2) = A_{1,2}(0)/(1 - q^2/m_A^2)$ and $V(q^2) = V(0)/(1 - q^2/m_V^2)$, and the pole mass m_V and m_A are fixed to $m_{D_s^*} \simeq 2.1\,\mathrm{GeV}/c^2$ and $m_{D_{s1}} \simeq 2.5\,\mathrm{GeV}/c^2$, respectively. The FF $A_1(q^2)$ is common to all three helicity amplitudes. Therefore, it is natural to define the two coupling constants, $r_V = V(0)/A_1(0)$ and $r_2 = A_2(0)/A_1(0)$ as FF ratios at the momentum square $q^2 = 0$. They are determined from the PWA fit.

The amplitude of the P-wave resonance $\mathcal{A}(m)$ is expressed as a relativistic Breit-Wigner

$$\mathcal{A}(m) = \frac{m_0\Gamma_0(p^*/p_0^*)}{m_0^2 - m^2 - im_0\Gamma(m)}\frac{B(p^*)}{B(p_0^*)}, \tag{7.4}$$

where $B(p) = 1/\sqrt{1 + r_{\mathrm{BW}}^2 p^2}$ with $r_{\mathrm{BW}} = 3.0\,(\mathrm{GeV}/c)^{-1}$ and $\Gamma(m) = \Gamma_0\left(\frac{p^*}{p_0^*}\right)^3\left(\frac{m_0}{m}\right)\left[\frac{B(p^*)}{B(p_0^*)}\right]^2$, where p_0^* is the modulus of the momentum of the K^- at the pole mass of the resonance m_0.

The S-wave contribution, characterized by the FF $\mathcal{F}_{10}$, is parametrized, assuming only $f_0(980)$ production, as

$$\mathcal{F}_{10} = p_{K^+K^-}m_{D_s}\frac{1}{1 - \frac{q^2}{m_A^2}}\mathcal{A}_S(m), \tag{7.5}$$

where $p_{K^+K^-}$ is the modulus of the momentum of the K^+K^- system in the D_s^+ rest frame. Here the term $\mathcal{A}_S(m)$ corresponds to the mass-dependent S-wave amplitude. The Flatté formula is used for the $f_0(980)$ contribution,

$$\mathcal{A}_S(m) = \frac{a_S e^{i\delta_S}}{m_0^2 - m^2 - i(g_1\rho_{\pi\pi} + g_2\rho_{KK})}, \tag{7.6}$$

where a_S and δ_S are the magnitude and phase of the S-wave amplitude; they are relative to the $D_s^+ \to \phi\mu^+\nu_\mu$ amplitude. The parameters g_1 and g_2 are taken from ref. [56]; $\rho_{\pi\pi}$ and ρ_{KK} are the phase-space (PHSP) factors for the decay channels $\pi\pi$ and KK, respectively.

7.2 Fit method

The PWA fit is performed using an unbinned maximum likelihood method. For one candidate event, the probability density function (PDF) can be expressed as:

$$\mathrm{PDF}(\xi,\eta) = (1 - f_b)\mathcal{S} + f_b\mathcal{B} = (1 - f_b)\frac{\omega(\xi,\eta)\,\epsilon(\xi)}{\int d\xi\,\omega(\xi,\eta)\,\epsilon(\xi)} + f_b\frac{B(\xi)}{\int d\xi\,B(\xi)}, \tag{7.7}$$

JHEP12(2023)072

where ξ denotes the five kinematic variables characterizing of one event and η denotes the fit parameters such as r_V and r_2; $\omega(\xi,\eta)$ is the decay intensity, and $B(\xi)$ is a function that describes the background; $\epsilon(\xi)$ is the reconstruction efficiency for the final state ξ and f_b is the fraction of background events. The above PDF can be rewritten as:

$$\mathrm{PDF}(\xi,\eta) = (1-f_b)\mathcal{S} + f_b\mathcal{B} = \epsilon(\xi)\left[(1-f_b)\frac{\omega(\xi,\eta)}{\int d\xi\,\omega(\xi,\eta)\,\epsilon(\xi)} + f_b\frac{B_\epsilon(\xi)}{\int d\xi\,B_\epsilon(\xi)\,\epsilon(\xi)}\right], \quad (7.8)$$

where $B_\epsilon(\xi)$ is defined to be the background distribution corrected by the acceptance function $\epsilon(\xi)$ [57]. By factorizing $\epsilon(\xi)$ out as a common factor, it becomes a part of the normalization. Then the likelihood is the product of probabilities of all the events:

$$\mathcal{L} = \prod_{i=1}^{N}\mathrm{PDF}(\xi_i,\eta) = \prod_{i=1}^{N}\epsilon(\xi_i)\left[(1-f_b)\frac{\omega(\xi_i,\eta)}{\int d\xi_i\,\omega(\xi_i,\eta)\,\epsilon(\xi_i)} + f_b\frac{B_\epsilon(\xi_i)}{\int d\xi_i\,B_\epsilon(\xi_i)\,\epsilon(\xi_i)}\right]. \quad (7.9)$$

In the fit, we optimize the parameters η by performing a minimization of a negative log-likelihood (NLL):

$$-\ln\mathcal{L} = -\sum_{i=1}^{N}\ln(\epsilon(\xi_i)) - \sum_{i=1}^{N}\ln\left[(1-f_b)\frac{\omega(\xi_i,\eta)}{\int d\xi_i\,\omega(\xi_i,\eta)\,\epsilon(\xi_i)} + f_b\frac{B_\epsilon(\xi_i)}{\int d\xi_i\,B_\epsilon(\xi_i)\,\epsilon(\xi_i)}\right]. \quad (7.10)$$

The first term in eq. (7.10) depends only on the events and efficiency, and remains constant during the fit. So actually we only compute the second term while performing the fit. Let σ_S be $\int d\xi_i\omega(\xi_i,\eta)\epsilon(\xi_i)$ and σ_B be $\int d\xi_i B_\epsilon(\xi_i)\epsilon(\xi_i)$. We minimize NLL:

$$\mathrm{NLL} = -\sum_{i=1}^{N}\ln\left[(1-f_b)\frac{\omega(\xi_i,\eta)}{\sigma_S} + f_b\frac{B_\epsilon(\xi)}{\sigma_B}\right]. \quad (7.11)$$

The acceptance efficiency has been considered in the calculation of the normalization integral factors σ_S and σ_B, which we calculate with MC integration using the signal MC. The normalization integral terms can be given as:

$$\sigma_S = \int d\xi_i\,\omega(\xi_i,\eta)\,\epsilon(\xi_i) \propto \frac{1}{N_{\mathrm{selected}}}\sum_{k=1}^{N_{\mathrm{selected}}}\frac{\omega(\xi_k,\eta)}{\omega(\xi_k,\eta_0)}, \quad (7.12)$$

$$\sigma_B = \int d\xi_i\,B_\epsilon(\xi_i)\,\epsilon(\xi_i) \propto \frac{1}{N_{\mathrm{selected}}}\sum_{k=1}^{N_{\mathrm{selected}}}\frac{B_\epsilon(\xi_k)}{\omega(\xi_k,\eta_0)}. \quad (7.13)$$

Here the terms η and η_0 represent the values of the parameters used in the fit and those used to produce the simulated events, respectively, while N_{selected} denotes the number of the signal MC events after reconstruction and selection.

A correction γ_ϵ is introduced to account for the potential bias caused by the tracking and PID efficiency differences between data and MC simulations. By weighting each signal MC event with γ_ϵ, the MC integration is given by

$$\sigma_S = \int d\xi_i\,\omega(\xi_i,\eta)\,\epsilon(\xi_i) \propto \frac{1}{N_{\mathrm{selected}}}\sum_{k=1}^{N_{\mathrm{selected}}}\frac{\omega(\xi_k,\eta)\,\gamma_\epsilon(\xi_k)}{\omega(\xi_k,\eta_0)}. \quad (7.14)$$

JHEP12(2023)072

The background shape is modeled with the inclusive MC and its fraction f_b is fixed according to the result of the $U_{\rm miss}$ fit. We model the background with non-parametric functions belonging to the class RooNDKeysPDF that use an adaptive kernel-estimation algorithm [58]. The value of $\epsilon(\xi_i)$ is obtained by calculating the ratio between the numbers of selected and truth events using PHSP MC samples, which are divided into $3\times5\times4\times5\times3$ bins in the five-variable space $(m^2, q^2, \theta_{K^-}, \theta_\mu, \chi)$. For some edge bins, we merge neighboring bins until twenty events are accumulated.

The data samples from the entire energy interval $[4.128, 4.226]$ GeV are divided into two groups: one group is $E_{\rm CM} = 4.178$ GeV, while the other combines the intervals $E_{\rm CM} \in [4.128, 4.157]$ GeV and $E_{\rm CM} \in [4.189, 4.226]$ GeV. The reason for combining the latter intervals is their low statistics. A simultaneous fit is performed to the two groups with the combined likelihood function:

$$\mathcal{L}^{ab} = \mathcal{L}^a(\xi|\eta)\mathcal{L}^b(\xi|\eta) = \prod_{i=1}^{n} \mathrm{PDF}^a(\xi_i|\eta) \prod_{j=1}^{m} \mathrm{PDF}^b(\xi_j|\eta), \tag{7.15}$$

where ξ and η are defined as before and a, b denote the likelihood values for the two data groups mentioned above.

7.3 PWA results

A simultaneous PWA fit is performed on the two data groups. The structure of the K^+K^- system is dominated by the vector meson ϕ; nevertheless, the S-wave contribution from the $f_0(980)$ has been considered but no significant contribution has been observed and the effect of $f_0(980)$ on the central solution is negligible. Therefore, only the ϕ in the K^+K^- system is considered in the nominal solution. In the fit, the mass and width of ϕ are fixed to the PDG values [45]. The FF ratios $r_V = \frac{V(0)}{A_1(0)} = 1.58 \pm 0.17 \pm 0.02$ and $r_2 = \frac{A_2(0)}{A_1(0)} = 0.71 \pm 0.14 \pm 0.02$ are obtained, with a correlation coefficient $\rho_{r_V, r_2} = -0.29$, where the first uncertainties are statistical and the second ones are systematic, see section 8 for their derivation. The projections of the five kinematic variables for the data are shown in figure 3.

A possible $f_0(980)$ component, an S-wave contribution to the $\mathcal{F}_{10}$ term, is studied by adding it to the nominal solution, where the $f_0(980)$ is parameterized with the Flatté formula and the parameters are fixed based on the BES measurement [56]. The statistical significance of this component is only 2.2σ as determined by the change of $-2\ln\mathcal{L}$ in the PWA fits with and without this component, taking into account the change of the number of degrees of freedom. The systematic uncertainty on the $f_0(980)$ is estimated as 0.28%, similar to the central value. By scanning the magnitude of the $f_0(980)$ component, the posterior probability variation of the expected BF is obtained and shown in figure 4. To take the systematic uncertainty into account, the posterior probability is convolved with a Gaussian function with a width equal to the systematic uncertainty. The upper limit obtained is $\mathcal{B}(D_s^+ \to f_0(980)\mu^+\nu_\mu) \cdot \mathcal{B}(f_0(980) \to K^+K^-) < 5.45 \times 10^{-4}$ at 90% credibility level.

JHEP12(2023)072

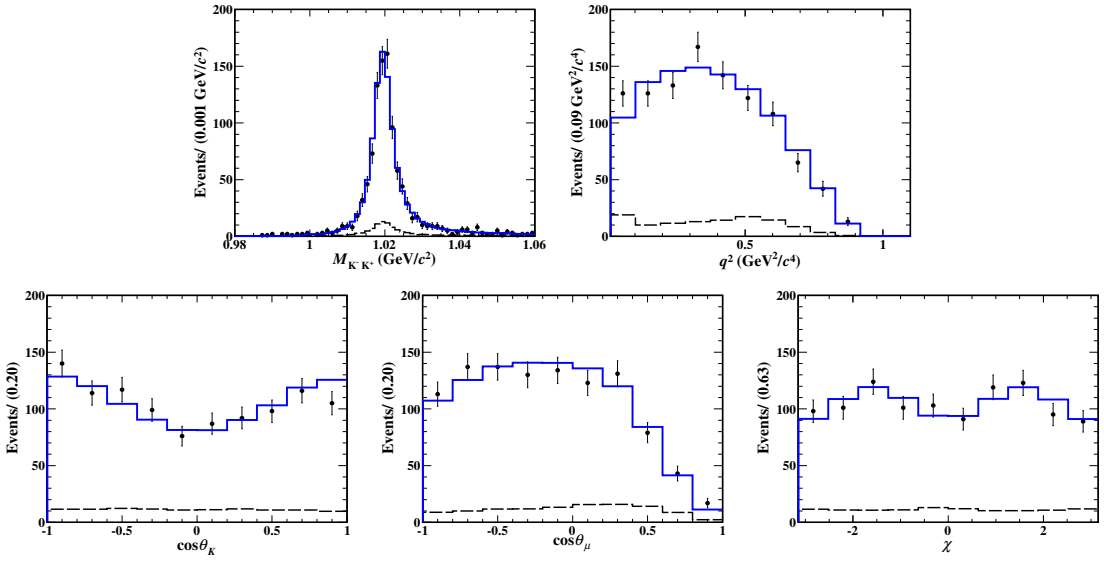

Figure 3. Projections of the data and simultaneous PWA fit onto the five kinematic variables for $D_s^+ \to K^+K^-\mu^+\nu_\mu$. The dots with error bars are data, the blue lines are the best fit, and the dashed lines show the sum of the simulated background contributions.

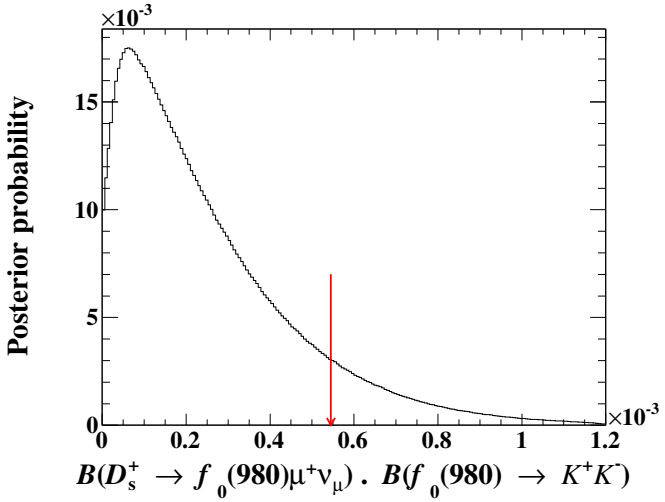

Figure 4. Posterior probability versus the product of $\mathcal{B}(D_s^+ \to f_0(980)\mu^+\nu_\mu) \cdot \mathcal{B}(f_0(980) \to K^+K^-)$. The red arrow shows the upper limit at 90% credibility level.

8 Systematic uncertainties

8.1 Branching fraction measurement

The sources of systematic uncertainty in the BF measurement are discussed below:

- $N_{\rm ST}^{\rm tot}$. The uncertainty due to $N_{\rm ST}^{\rm tot}$ is mainly from the fits to the $M_{\rm tag}$ spectra. It is estimated by varying the signal and background shapes in the fits to data and inclusive MC sample. The alternative signal shape is obtained by varying the matching

JHEP12(2023)072

Source	Uncertainty (%)
$N_{\rm ST}^{\rm tot}$	0.5
Tracking of $K^{\pm}$	1.8
PID of $K^{\pm}$	0.8
Tracking of μ^{+}	0.3
PID of μ^{+}	0.4
Selection of transition $\gamma(\pi^0)$	1.0
Tag bias	0.1
$E_{\rm extra\gamma}^{\rm max}$, $N_{\rm extra}^{\rm char}$ and $N_{\rm extra}^{\pi^0}$	0.4
$M_{\phi\nu_\mu}$ and $M_{\phi\mu^+}$	1.0
$U_{\rm miss}$ fit	1.6
Least $\lvert\Delta E\rvert$	0.4
MC statistics	0.2
MC model	0.8
Quoted BF	1.0
Total	3.3

Table 3. Relative systematic uncertainties in the BF measurement.

requirement between generated and reconstructed angles from 15° to 10° and 20°. The alternative background shape is obtained by replacing the nominal shape to be a third order polynomial function. The difference of the ST total efficiency-corrected yields in data is taken as systematic uncertainty. The uncertainty arising from the background fluctuation of the total ST yield is considered as a systematic uncertainty. Adding these three terms in quadrature gives the systematic uncertainty in $N_{\rm ST}^{\rm tot}$ to be 0.5%.

- $K^{\pm}$ tracking/PID efficiency. The uncertainties in the tracking and PID efficiencies of $K^{\pm}$ are studied with a control sample of $e^+e^- \to K^+K^-\pi^+\pi^-$. The momentum-weighted data-MC differences are 1.008 ± 0.009 (1.009 ± 0.009) and 1.001 ± 0.004 (0.998 ± 0.004) arising from K^+ (K^-) tracking and PID efficiencies, respectively. The signal efficiencies applied to data are corrected by these factors. The uncertainties on these corrections are taken as the systematic uncertainties due to $K^{\pm}$ tracking and $K^{\pm}$ PID, as listed in table 3.
- μ^+ tracking/PID efficiency. The μ^+ tracking and PID efficiencies are studied with a control sample of $e^+e^- \to \gamma\mu^+\mu^-$. The data-MC differences are 0.987 ± 0.003 for μ^+ tracking and 1.040 ± 0.004 for μ^+ PID efficiencies. We correct the signal efficiencies to data by these factors. The uncertainties on these corrections are taken as the systematic uncertainties due to μ^+ tracking and μ^+ PID, as listed in table 3.
- Transition $\gamma(\pi^0)$ reconstruction. The efficiencies of the $\gamma(\pi^0)$ reconstruction have been investigated with the control samples of $J/\psi \to \pi^+\pi^-\pi^0$ ($e^+e^- \to$

JHEP12(2023)072

$K^+K^-\pi^+\pi^-\pi^0$). The systematic uncertainty of the $\gamma(\pi^0)$ selection is assigned to be 1.0% in this analysis.

- Tag bias. The ST efficiencies determined from the inclusive MC sample and those from the signal MC sample may be different, which may cause an uncertainty associated with the ST selection, called tag bias. With the tracking and PID efficiencies for kaons and pions with different track multiplicities, the average difference, 0.1%, is assigned as the systematic uncertainty due to tag bias.
- $E^{\rm max}_{{\rm extra}\gamma}$, $N^{\rm char}_{\rm extra}$ and $N^{\pi^0}_{\rm extra}$. The systematic uncertainty in the $E^{\rm max}_{{\rm extra}\gamma}$, $N^{\rm char}_{\rm extra}$, and $N^{\pi^0}_{\rm extra}$ is estimated to be 0.4% with the DT hadronic sample of $D_s^+ \to K^+K^-\pi^+$, a mode with tracks similar to the signal decay. The differences of the efficiencies between the data and MC simulation is 1.035 ± 0.004. After correcting the MC efficiency by this factor, we take 0.4% as the systematic uncertainty.
- $M_{\phi\nu_\mu}$ and $M_{\phi\mu^+}$. The uncertainties of the $M_{\phi\nu_\mu}$ and $M_{\phi\mu^+}$ requirements are estimated with a control sample of $D_s^+ \to \phi e^+\nu_e$, and the difference of the efficiencies between the data and MC simulation of 1.0% is taken as the uncertainty.
- $U_{\rm miss}$ fit. The uncertainty related to the $U_{\rm miss}$ fit is estimated with alternative signal and background shapes. The systematic uncertainty from the signal shape is estimated by varying the ρ parameter of RooNDKeysPDF from 1 to 2; this increases the smoothing. The systematic uncertainty due to the background shape is studied by varying the relative fractions of the major backgrounds from $e^+e^- \to q\bar{q}$ and the non-$D_s^{*+}D_s^-$ open charm processes by $\pm30\%$, based on the errors of input cross sections in the inclusive MC sample. Quadratic sum of the change of the fitted signal yield for each item, 1.6%, is assigned as the systematic uncertainty in the $U_{\rm miss}$ fit.
- Least $|\Delta E|$. To estimate the systematic uncertainty in the least $|\Delta E|$ method in the selection of the transition $\gamma(\pi^0)$ from D_s^{*+}, we use the control samples of $D_s^+ \to K^+K^-\pi^+$ and $D_s^+ \to \eta\pi^0\pi^+$. The difference in the efficiencies of selecting the transition $\gamma(\pi^0)$ candidates between data and MC simulation, 0.4%, is assigned as the uncertainty.
- MC statistics. The uncertainty due to MC statistics, 0.2%, is assigned as a systematic uncertainty.
- MC model. The systematic uncertainty of MC model is estimated by comparing the signal efficiency obtained with the alternative signal MC samples generated by varying the input FF ratios by $\pm1\sigma$ statistical error. The larger change of the signal efficiency, 0.8%, is taken as the corresponding uncertainty.
- Quoted BF. The uncertainty of the quoted BF of $\phi \to K^+K^-$ is 1.0% [45]. We have also examined the averaged signal efficiency by varying the quoted BFs of $D_s^{*+} \to \gamma D_s^+$ and $D_s^{*+} \to \pi^0 D_s^+$ within $\pm1\sigma$ and find the change of the signal efficiency is less than 0.2%. Adding these two items in quadrature gives the total systematic uncertainty due to the quoted BFs to be 1.0%.

The above sources are summarized in table 3. The total systematic uncertainty, obtained by summing the contributions in quadrature, is 3.3%.

JHEP12(2023)072

Source	r_V	r_2
Background estimation	0.31%	0.49%
$r_{\rm BW}$	0.06%	0.28%
m_V	0.95%	0.03%
m_A	1.10%	2.39%
ϕ line shape	0.01%	0.07%
Efficiency corrections	0.13%	0.28%
Total	1.46%	2.47%

Table 4. Relative systematic uncertainties of the measurements of the FF ratios.

8.2 Measurement of form factors

The following sources of systematic uncertainties, summarized in table 4, have been considered in the FF ratio measurements:

- Background estimation. First, the fractions of backgrounds for the two sample groups, i.e. f_b in eq. (7.11), are varied by their corresponding statistical uncertainties, addressing background levels. Second, an alternative MC-simulated shape is used to examine the uncertainty arising from the background shape modeling. Alternative background shapes are obtained with the relative fractions of the backgrounds from $e^+e^- \to q\bar{q}$ and non-$D_s^{*+}D_s^-$ varied by the statistical uncertainties of their cross sections. The differences caused by these variations are assigned as the uncertainties.
- $r_{\rm BW}$. The effective radius of the resonance is set to $3.0\,(\mathrm{GeV}/c)^{-1}$ in the nominal fit. This value is varied from $1.0\,(\mathrm{GeV}/c)^{-1}$ to $5.0\,(\mathrm{GeV}/c)^{-1}$, taking the largest difference in the results as the systematic uncertainties.
- m_V and m_A. The fixed parameters m_V and m_A are varied by $\pm 100\,\mathrm{MeV}/c^2$ to estimate the uncertainties associated with the pole mass assumption. The differences from the nominal result are assigned as systematic uncertainties.
- ϕ line shape. The uncertainty is estimated by varying the mass and width of the ϕ meson by $\pm 1\sigma$; the largest difference is taken as systematic uncertainty.
- Efficiency corrections. These corrections compensate for efficiency differences between data and MC simulation from PID and tracking, reflected in the γ_ϵ parameters in eq. (7.14). The uncertainties due to the γ_ϵ parameters are obtained by performing the PWA while varying PID and tracking efficiencies by their uncertainties. The difference from the nominal result is assigned as systematic uncertainty.

9 Summary

A PWA is performed on the SL decay $D_s^+ \to K^+K^-\mu^+\nu_\mu$ for the first time using $7.33\,\mathrm{fb}^{-1}$ of e^+e^- collision data collected by the BESIII detector at $E_{\rm CM}$ in the range from 4.128 GeV

JHEP12(2023)072

Experiments	r_V	r_2
PDG [45]	1.80 ± 0.08	0.84 ± 0.11
This analysis	$1.58 \pm 0.17 \pm 0.02$	$0.71 \pm 0.14 \pm 0.02$
BABAR [26]	$1.807 \pm 0.046 \pm 0.065$	$0.816 \pm 0.036 \pm 0.030$
FOCUS [59]	$1.549 \pm 0.250 \pm 0.148$	$0.713 \pm 0.202 \pm 0.284$
Theory	r_V	r_2
CCQM [5]	1.34 ± 0.27	0.99 ± 0.20
CQM [6]	1.72	0.73
LFQM [7]	1.42	0.86
LQCD [3]	1.72 ± 0.21	0.74 ± 0.12
HMχT [8]	1.80	0.52

Table 5. Measured FF ratios and comparison with previous measurements.

to 4.226 GeV. The absolute BF of $D_s^+ \to \phi\mu^+\nu_\mu$ is measured as $(2.25 \pm 0.09 \pm 0.07) \times 10^{-2}$. The precision of the BF is a factor of 4.3 better than the world average value. Combining this result with the world average of $\mathcal{B}(D_s^+ \to \phi e^+\nu_e)$ [45], the ratio of the two BFs obtained is $\mathcal{B}(D_s^+ \to \phi\mu^+\nu_\mu)/\mathcal{B}(D_s^+ \to \phi e^+\nu_e) = 0.94 \pm 0.08$, consistent with the SM prediction. Assuming that the only S-wave contribution is from the $f_0(980)$, the process of $D_s^+ \to f_0(980)\mu^+\nu_\mu$, $f_0(980) \to K^+K^-$ was searched for and no significant signal was found. The upper limit $\mathcal{B}(D_s^+ \to f_0(980)\mu^+\nu_\mu) \cdot \mathcal{B}(f_0(980) \to K^+K^-) < 5.45 \times 10^{-4}$ is set at the 90% credibility level.

By assuming only the ϕ contribution, the FF ratios $r_V = \frac{V(0)}{A_1(0)} = 1.58 \pm 0.17 \pm 0.02$ and $r_2 = \frac{A_2(0)}{A_1(0)} = 0.71 \pm 0.14 \pm 0.02$ are extracted. These FFs measurements are summarized in table 5 and compared to the previous measurements and the theoretical calculations.

These FF measurements are consistent with the *BABAR* [26] and FOCUS [59] measurements. The obtained FF ratios confirm the theoretical predictions [3, 5–7], which have been used in the determination of $|V_{cs}|$ and CKM unitarity tests.

Acknowledgments

The BESIII collaboration thanks the staff of BEPCII and the IHEP computing center for their strong support. The authors thank Prof. Yao Yu for helpful discussions. This work is supported in part by National Key R&D Program of China under Contracts Nos. 2020YFA0406400, 2020YFA0406300; National Natural Science Foundation of China (NSFC) under Contracts Nos. 11805037, 11635010, 11735014, 11835012, 11935015, 11935016, 11935018, 11961141012, 12022510, 12025502, 12035009, 12035013, 12061131003, 12192260, 12192261, 12192262, 12192263, 12192264, 12192265, 12221005, 12225509, 12235017; Guangdong Basic and Applied Basic Research Foundation under Grant No. 2023A1515010121; the Chinese Academy of Sciences (CAS) Large-Scale Scientific Facility Program; Joint Large-Scale Scientific Facility Funds of the NSFC and

JHEP12(2023)072

CAS under Contracts No. U2032104; the CAS Center for Excellence in Particle Physics (CCEPP); CAS Key Research Program of Frontier Sciences under Contracts Nos. QYZDJ-SSW-SLH003, QYZDJ-SSW-SLH040; 100 Talents Program of CAS; The Institute of Nuclear and Particle Physics (INPAC) and Shanghai Key Laboratory for Particle Physics and Cosmology; ERC under Contract No. 758462; European Union's Horizon 2020 research and innovation programme under Marie Sklodowska-Curie grant agreement under Contract No. 894790; German Research Foundation DFG under Contracts Nos. 443159800, 455635585, Collaborative Research Center CRC 1044, FOR5327, GRK 2149; Istituto Nazionale di Fisica Nucleare, Italy; Ministry of Development of Turkey under Contract No. DPT2006K-120470; National Research Foundation of Korea under Contract No. NRF-2022R1A2C1092335; National Science and Technology fund of Mongolia; National Science Research and Innovation Fund (NSRF) via the Program Management Unit for Human Resources & Institutional Development, Research and Innovation of Thailand under Contract No. B16F640076; Polish National Science Centre under Contract No. 2019/35/O/ST2/02907; The Swedish Research Council; U.S. Department of Energy under Contract No. DE-FG02-05ER41374.

References

[1] H. Na, C.T.H. Davies, E. Follana, J. Koponen, G.P. Lepage and J. Shigemitsu, *$D \to \pi, l\nu$ Semileptonic Decays, $|V_{cd}|$ and 2^{nd} Row Unitarity from Lattice QCD*, *Phys. Rev. D* **84** (2011) 114505 [arXiv:1109.1501] [INSPIRE].

[2] S. Aoki et al., *Review of lattice results concerning low-energy particle physics*, *Eur. Phys. J. C* **77** (2017) 112 [arXiv:1607.00299] [INSPIRE].

[3] HPQCD collaboration, *V_{cs} from $D_s \to \phi l\nu$ semileptonic decay and full lattice QCD*, *Phys. Rev. D* **90** (2014) 074506 [arXiv:1311.6669] [INSPIRE].

[4] HPQCD collaboration, *D_s to ϕ and other transitions from lattice QCD*, *PoS* **LATTICE2013** (2014) 390 [arXiv:1311.6967] [INSPIRE].

[5] N.R. Soni, M.A. Ivanov, J.G. Körner, J.N. Pandya, P. Santorelli and C.T. Tran, *Semileptonic $D_{(s)}$-meson decays in the light of recent data*, *Phys. Rev. D* **98** (2018) 114031 [arXiv:1810.11907] [INSPIRE].

[6] D. Melikhov and B. Stech, *Weak form-factors for heavy meson decays: An Update*, *Phys. Rev. D* **62** (2000) 014006 [hep-ph/0001113] [INSPIRE].

[7] R.C. Verma, *Decay constants and form factors of s-wave and p-wave mesons in the covariant light-front quark model*, *J. Phys. G* **39** (2012) 025005 [arXiv:1103.2973] [INSPIRE].

[8] S. Fajfer and J.F. Kamenik, *Charm meson resonances and $D \to V$ semileptonic form-factors*, *Phys. Rev. D* **72** (2005) 034029 [hep-ph/0506051] [INSPIRE].

[9] LHCb collaboration, *Test of lepton universality in beauty-quark decays*, *Nat. Phys.* **18** (2022) 277 [*Addendum ibid.* **19** (2023) 1517] [arXiv:2103.11769] [INSPIRE].

JHEP12(2023)072

[10] LHCb collaboration, *Measurement of lepton universality parameters in $B^+ \to K^+\ell^+\ell^-$ and $B^0 \to K^{*0}\ell^+\ell^-$ decays*, *Phys. Rev. D* **108** (2023) 032002 [arXiv:2212.09153] [INSPIRE].

[11] M. Bauer and M. Neubert, *Minimal Leptoquark Explanation for the $R_{D^{(*)}}$, R_K, and $(g-2)_\mu$ Anomalies*, *Phys. Rev. Lett.* **116** (2016) 141802 [arXiv:1511.01900] [INSPIRE].

[12] A. Crivellin, J. Heeck and P. Stoffer, *A perturbed lepton-specific two-Higgs-doublet model facing experimental hints for physics beyond the Standard Model*, *Phys. Rev. Lett.* **116** (2016) 081801 [arXiv:1507.07567] [INSPIRE].

[13] A. Crivellin, G. D'Ambrosio and J. Heeck, *Explaining $h \to \mu^\pm\tau^\mp$, $B \to K^*\mu^+\mu^-$ and $B \to K\mu^+\mu^-/B \to Ke^+e^-$ in a two-Higgs-doublet model with gauged $L_\mu - L_\tau$*, *Phys. Rev. Lett.* **114** (2015) 151801 [arXiv:1501.00993] [INSPIRE].

[14] S. Fajfer, J.F. Kamenik, I. Nisandzic and J. Zupan, *Implications of Lepton Flavor Universality Violations in B Decays*, *Phys. Rev. Lett.* **109** (2012) 161801 [arXiv:1206.1872] [INSPIRE].

[15] S. Fajfer, J.F. Kamenik and I. Nisandzic, *On the $B \to D^*\tau\bar{\nu}_\tau$ Sensitivity to New Physics*, *Phys. Rev. D* **85** (2012) 094025 [arXiv:1203.2654] [INSPIRE].

[16] BESIII collaboration, *Measurement of the branching fraction for the semi-leptonic decay $D^{0(+)} \to \pi^{-(0)}\mu^+\nu_\mu$ and test of lepton universality*, *Phys. Rev. Lett.* **121** (2018) 171803 [arXiv:1802.05492] [INSPIRE].

[17] BESIII collaboration, *Study of the $D^0 \to K^-\mu^+\nu_\mu$ Dynamics and Test of Lepton Flavor Universality with $D^0 \to K^-\ell^+\nu_\ell$ Decays*, *Phys. Rev. Lett.* **122** (2019) 011804 [arXiv:1810.03127] [INSPIRE].

[18] BESIII collaboration, *First Observation of $D^+ \to \eta\mu^+\nu_\mu$ and Measurement of Its Decay Dynamics*, *Phys. Rev. Lett.* **124** (2020) 231801 [arXiv:2003.12220] [INSPIRE].

[19] BESIII collaboration, *Measurement of the Dynamics of the Decays $D_s^+ \to \eta^{(\prime)}e^+\nu_e$*, *Phys. Rev. Lett.* **122** (2019) 121801 [arXiv:1901.02133] [INSPIRE].

[20] BESIII collaboration, *Measurements of the branching fractions for the semi-leptonic decays $D_s^+ \to \phi e^+\nu_e$, $\phi\mu^+\nu_\mu$, $\eta\mu^+\nu_\mu$ and $\eta'\mu^+\nu_\mu$*, *Phys. Rev. D* **97** (2018) 012006 [arXiv:1709.03680] [INSPIRE].

[21] B.-C. Ke, J. Koponen, H.-B. Li and Y. Zheng, *Recent Progress in Leptonic and Semileptonic Decays of Charmed Hadrons*, *Ann. Rev. Nucl. Part. Sci.* **73** (2023) 285 [arXiv:2310.05228] [INSPIRE].

[22] BESIII collaboration, *First Measurement of the Absolute Branching Fraction of $\Lambda \to p\mu^-\bar{\nu}_\mu$*, *Phys. Rev. Lett.* **127** (2021) 121802 [arXiv:2107.06704] [INSPIRE].

[23] BELLE collaboration, *Measurements of the branching fractions of the semileptonic decays $\Xi_c^0 \to \Xi^-\ell^+\nu_\ell$ and the asymmetry parameter of $\Xi_c^0 \to \Xi^-\pi^+$*, *Phys. Rev. Lett.* **127** (2021) 121803 [arXiv:2103.06496] [INSPIRE].

[24] BELLE collaboration, *First test of lepton flavor universality in the charmed baryon decays $\Omega_c^0 \to \Omega^-\ell^+\nu_\ell$ using data of the Belle experiment*, *Phys. Rev. D* **105** (2022) L091101 [arXiv:2112.10367] [INSPIRE].

[25] BESIII collaboration, *Measurement of the absolute branching fraction for $\Lambda_c^+ \to \Lambda e^+\nu_e$*, *Phys. Rev. Lett.* **115** (2015) 221805 [arXiv:1510.02610] [INSPIRE].

JHEP12(2023)072

[26] BaBar collaboration, *Study of the decay $D_s^+ \to K^+K^-e^+\nu_e$*, *Phys. Rev. D* **78** (2008) 051101 [arXiv:0807.1599] [INSPIRE].

[27] H. Kim, K.S. Kim, M.-K. Cheoun, D. Jido and M. Oka, *Further signatures to support the tetraquark mixing framework for the two light-meson nonets*, *Phys. Rev. D* **99** (2019) 014005 [arXiv:1811.00187] [INSPIRE].

[28] Z.-Q. Wang, X.-W. Kang, J.A. Oller and L. Zhang, *Analysis on the composite nature of the light scalar mesons $f_0(980)$ and $a_0(980)$*, *Phys. Rev. D* **105** (2022) 074016 [arXiv:2201.00492] [INSPIRE].

[29] S. Stone and L. Zhang, *Use of $B \to J/\psi f_0$ decays to discern the $q\bar{q}$ or tetraquark nature of scalar mesons*, *Phys. Rev. Lett.* **111** (2013) 062001 [arXiv:1305.6554] [INSPIRE].

[30] D.-L. Yao, L.-Y. Dai, H.-Q. Zheng and Z.-Y. Zhou, *A review on partial-wave dynamics with chiral effective field theory and dispersion relation*, *Rept. Prog. Phys.* **84** (2021) 076201 [arXiv:2009.13495] [INSPIRE].

[31] L.-Y. Dai and M.R. Pennington, *Comprehensive amplitude analysis of $\gamma\gamma \to \pi^+\pi^-, \pi^0\pi^0$ and $\overline{K}K$ below 1.5 GeV*, *Phys. Rev. D* **90** (2014) 036004 [arXiv:1404.7524] [INSPIRE].

[32] BESIII collaboration, *Design and Construction of the BESIII Detector*, *Nucl. Instrum. Meth. A* **614** (2010) 345 [arXiv:0911.4960] [INSPIRE].

[33] C. Yu et al., *BEPCII Performance and Beam Dynamics Studies on Luminosity*, in the proceedings of the *7th International Particle Accelerator Conference (IPAC 2016)*, Busan, Republic of Korea, 8–13 May 2016 [DOI:10.18429/JACoW-IPAC2016-TUYA01] [INSPIRE].

[34] BESIII collaboration, *Future Physics Programme of BESIII*, *Chin. Phys. C* **44** (2020) 040001 [arXiv:1912.05983] [INSPIRE].

[35] H.-B. Li and X.-R. Lyu, *Study of the standard model with weak decays of charmed hadrons at BESIII*, *Natl. Sci. Rev.* **8** (2021) nwab181 [arXiv:2103.00908] [INSPIRE].

[36] K.-X. Huang et al., *Method for detector description transformation to Unity and application in BESIII*, *Nucl. Sci. Tech.* **33** (2022) 142 [arXiv:2206.10117] [INSPIRE].

[37] P. Cao et al., *Design and construction of the new BESIII endcap Time-of-Flight system with MRPC Technology*, *Nucl. Instrum. Meth. A* **953** (2020) 163053 [INSPIRE].

[38] BESIII collaboration, *Measurement of integrated luminosities at BESIII for data samples at center-of-mass energies between 4.0 and 4.6 GeV*, *Chin. Phys. C* **46** (2022) 113002 [arXiv:2203.03133] [INSPIRE].

[39] BESIII collaboration, *Observation of the decay $D_s^+ \to \omega\pi^+\eta$*, *Phys. Rev. D* **107** (2023) 052010 [arXiv:2302.04670] [INSPIRE].

[40] GEANT4 collaboration, *GEANT4 — a simulation toolkit*, *Nucl. Instrum. Meth. A* **506** (2003) 250 [INSPIRE].

[41] S. Jadach, B.F.L. Ward and Z. Was, *Coherent exclusive exponentiation for precision Monte Carlo calculations*, *Phys. Rev. D* **63** (2001) 113009 [hep-ph/0006359] [INSPIRE].

[42] R.-G. Ping, *An exclusive event generator for e^+e^- scan experiments*, *Chin. Phys. C* **38** (2014) 083001 [arXiv:1309.3932] [INSPIRE].

[43] D.J. Lange, *The EvtGen particle decay simulation package*, *Nucl. Instrum. Meth. A* **462** (2001) 152 [INSPIRE].

[44] R.-G. Ping, *Event generators at BESIII*, *Chin. Phys. C* **32** (2008) 599 [INSPIRE].

JHEP12(2023)072

[45] Particle Data collaboration, *Review of Particle Physics*, *Prog. Theor. Exp. Phys.* **2022** (2022) 083C01 [INSPIRE].

[46] J.C. Chen, G.S. Huang, X.R. Qi, D.H. Zhang and Y.S. Zhu, *Event generator for J/ψ and $\psi(2S)$ decay*, *Phys. Rev. D* **62** (2000) 034003 [INSPIRE].

[47] R.-L. Yang, R.-G. Ping and H. Chen, *Tuning and Validation of the Lundcharm Model with J/ψ Decays*, *Chin. Phys. Lett.* **31** (2014) 061301 [INSPIRE].

[48] E. Richter-Was, *QED bremsstrahlung in semileptonic B and leptonic tau decays*, *Phys. Lett. B* **303** (1993) 163 [INSPIRE].

[49] BESIII collaboration, *Measurement of the absolute branching fractions for purely leptonic D_s^+ decays*, *Phys. Rev. D* **104** (2021) 052009 [arXiv:2102.11734] [INSPIRE].

[50] MARK-III collaboration, *Direct Measurements of Charmed d Meson Hadronic Branching Fractions*, *Phys. Rev. Lett.* **56** (1986) 2140 [INSPIRE].

[51] BESIII collaboration, *Determination of the pseudoscalar decay constant $f_{D_s^+}$ via $D_s^+ \to \mu^+\nu_\mu$*, *Phys. Rev. Lett.* **122** (2019) 071802 [arXiv:1811.10890] [INSPIRE].

[52] BESIII collaboration, *Search for the decay $D_s^+ \to \gamma e^+\nu_e$*, *Phys. Rev. D* **99** (2019) 072002 [arXiv:1902.03351] [INSPIRE].

[53] N. Cabibbo and A. Maksymowicz, *Angular Correlations in K_{e4} Decays and Determination of Low-Energy $\pi - \pi$ Phase Shifts*, *Phys. Rev.* **137** (1965) B438 [*Erratum ibid.* **168** (1968) 1926] [INSPIRE].

[54] C.L.Y. Lee, M. Lu and M.B. Wise, *B_{l4} and D_{l4} decay*, *Phys. Rev. D* **46** (1992) 5040 [INSPIRE].

[55] H. Zhang, B.-C. Ke, Y. Yu and E. Wang, *Lepton mass correction in partial wave analyses of charmed meson semi-leptonic decays*, *Chin. Phys. C* **47** (2023) 063101 [arXiv:2302.10541] [INSPIRE].

[56] BES collaboration, *Resonances in $J/\psi \to \phi\pi^+\pi^-$ and ϕK^+K^-*, *Phys. Lett. B* **607** (2005) 243 [hep-ex/0411001] [INSPIRE].

[57] CLEO collaboration, *Amplitude analysis of $D^0 \to K^+K^-\pi^+\pi^-$*, *Phys. Rev. D* **85** (2012) 122002 [arXiv:1201.5716] [INSPIRE].

[58] K.S. Cranmer, *Kernel estimation in high-energy physics*, *Comput. Phys. Commun.* **136** (2001) 198 [hep-ex/0011057] [INSPIRE].

[59] FOCUS collaboration, *New measurements of the $D_s^+ \to \phi\mu^+\nu_\mu$ form-factor ratios*, *Phys. Lett. B* **586** (2004) 183 [hep-ex/0401001] [INSPIRE].

JHEP12(2023)072

The BESIII collaboration

M. Ablikim[1], M.N. Achasov[13,b], P. Adlarson[75], X.C. Ai[81], R. Aliberti[36], A. Amoroso[74A,74C], M.R. An[40], Q. An[71,58], Y. Bai[57], O. Bakina[37], I. Balossino[30A], Y. Ban[47,g], V. Batozskaya[1,45], K. Begzsuren[33], N. Berger[36], M. Berlowski[45], M. Bertani[29A], D. Bettoni[30A], F. Bianchi[74A,74C], E. Bianco[74A,74C], J. Bloms[68], A. Bortone[74A,74C], I. Boyko[37], R.A. Briere[5], A. Brueggemann[68], H. Cai[76], X. Cai[1,58], A. Calcaterra[29A], G.F. Cao[1,63], N. Cao[1,63], S.A. Cetin[62A], J.F. Chang[1,58], T.T. Chang[77], W.L. Chang[1,63], G.R. Che[44], G. Chelkov[37,a], C. Chen[44], Chao Chen[55], G. Chen[1], H.S. Chen[1,63], M.L. Chen[1,58,63], S.J. Chen[43], S.M. Chen[61], T. Chen[1,63], X.R. Chen[32,63], X.T. Chen[1,63], Y.B. Chen[1,58], Y.Q. Chen[35], Z.J. Chen[26,h], W.S. Cheng[74C], S.K. Choi[10], X. Chu[44], G. Cibinetto[30A], S.C. Coen[4], F. Cossio[74C], J.J. Cui[50], H.L. Dai[1,58], J.P. Dai[79], A. Dbeyssi[19], R.E. de Boer[4], D. Dedovich[37], Z.Y. Deng[1], A. Denig[36], I. Denysenko[37], M. Destefanis[74A,74C], F. De Mori[74A,74C], B. Ding[66,1], X.X. Ding[47,g], Y. Ding[41], Y. Ding[35], J. Dong[1,58], L.Y. Dong[1,63], M.Y. Dong[1,58,63], X. Dong[76], S.X. Du[81], Z.H. Duan[43], P. Egorov[37,a], Y.L. Fan[76], J. Fang[1,58], S.S. Fang[1,63], W.X. Fang[1], Y. Fang[1], R. Farinelli[30A], L. Fava[74B,74C], F. Feldbauer[4], G. Felici[29A], C.Q. Feng[71,58], J.H. Feng[59], K. Fischer[69], M. Fritsch[4], C. Fritzsch[68], C.D. Fu[1], J.L. Fu[63], Y.W. Fu[1], H. Gao[63], Y.N. Gao[47,g], Yang Gao[71,58], S. Garbolino[74C], I. Garzia[30A,30B], P.T. Ge[76], Z.W. Ge[43], C. Geng[59], E.M. Gersabeck[67], A. Gilman[69], K. Goetzen[14], L. Gong[41], W.X. Gong[1,58], W. Gradl[36], S. Gramigna[30A,30B], M. Greco[74A,74C], M.H. Gu[1,58], Y.T. Gu[16], C.Y. Guan[1,63], Z.L. Guan[23], A.Q. Guo[32,63], L.B. Guo[42], M.J. Guo[50], R.P. Guo[49], Y.P. Guo[12,f], A. Guskov[37,a], T.T. Han[50], W.Y. Han[40], X.Q. Hao[20], F.A. Harris[65], K.K. He[55], K.L. He[1,63], F.H.H. Heinsius[4], C.H. Heinz[36], Y.K. Heng[1,58,63], C. Herold[60], T. Holtmann[4], P.C. Hong[12,f], G.Y. Hou[1,63], X.T. Hou[1,63], Y.R. Hou[63], Z.L. Hou[1], H.M. Hu[1,63], J.F. Hu[56,i], T. Hu[1,58,63], Y. Hu[1], G.S. Huang[71,58], K.X. Huang[59], L.Q. Huang[32,63], X.T. Huang[50], Y.P. Huang[1], T. Hussain[73], N. Hüsken[28,36], W. Imoehl[28], M. Irshad[71,58], J. Jackson[28], S. Jaeger[4], S. Janchiv[33], J.H. Jeong[10], Q. Ji[1], Q.P. Ji[20], X.B. Ji[1,63], X.L. Ji[1,58], Y.Y. Ji[50], X.Q. Jia[50], Z.K. Jia[71,58], P.C. Jiang[47,g], S.S. Jiang[40], T.J. Jiang[17], X.S. Jiang[1,58,63], Y. Jiang[63], J.B. Jiao[50], Z. Jiao[24], S. Jin[43], Y. Jin[66], M.Q. Jing[1,63], T. Johansson[75], X. Kui[1], S. Kabana[34], N. Kalantar-Nayestanaki[64], X.L. Kang[9], X.S. Kang[41], R. Kappert[64], M. Kavatsyuk[64], B.C. Ke[81], A. Khoukaz[68], R. Kiuchi[1], R. Kliemt[14], O.B. Kolcu[62A], B. Kopf[4], M.K. Kuessner[4], A. Kupsc[45,75], W. Kühn[38], J.J. Lane[67], P. Larin[19], A. Lavania[27], L. Lavezzi[74A,74C], T.T. Lei[71,k], Z.H. Lei[71,58], H. Leithoff[36], M. Lellmann[36], T. Lenz[36], C. Li[48], C. Li[44], C.H. Li[40], Cheng Li[71,58], D.M. Li[81], F. Li[1,58], G. Li[1], H. Li[71,58], H.B. Li[1,63], H.J. Li[20], H.N. Li[56,i], Hui Li[44], J.R. Li[61], J.S. Li[59], J.W. Li[50], K.L. Li[20], Ke Li[1], L.J. Li[1,63], L.K. Li[1], Lei Li[3], M.H. Li[44], P.R. Li[39,j,k], Q.X. Li[50], S.X. Li[12], T. Li[50], W.D. Li[1,63], W.G. Li[1], X.H. Li[71,58], X.L. Li[50], Xiaoyu Li[1,63], Y.G. Li[47,g], Z.J. Li[59], Z.X. Li[16], C. Liang[43], H. Liang[1,63], H. Liang[71,58], H. Liang[35], Y.F. Liang[54], Y.T. Liang[32,63], G.R. Liao[15], L.Z. Liao[50], J. Libby[27], A. Limphirat[60], D.X. Lin[32,63], T. Lin[1], B.J. Liu[1], B.X. Liu[76], C. Liu[35], C.X. Liu[1], F.H. Liu[53], Fang Liu[1], Feng Liu[6], G.M. Liu[56,i], H. Liu[39,j,k], H.B. Liu[16], H.M. Liu[1,63], Huanhuan Liu[1], Huihui Liu[22], J.B. Liu[71,58], J.L. Liu[72], J.Y. Liu[1,63], K. Liu[1], K.Y. Liu[41], Ke Liu[23], L. Liu[71,58], L.C. Liu[44], Lu Liu[44], M.H. Liu[12,f], P.L. Liu[1], Q. Liu[63], S.B. Liu[71,58], T. Liu[12,f], W.K. Liu[44], W.M. Liu[71,58], X. Liu[39,j,k], Y. Liu[39,j,k], Y. Liu[81], Y.B. Liu[44], Z.A. Liu[1,58,63], Z.Q. Liu[50], X.C. Lou[1,58,63], F.X. Lu[59], H.J. Lu[24], J.G. Lu[1,58], X.L. Lu[1], Y. Lu[7], Y.P. Lu[1,58], Z.H. Lu[1,63], C.L. Luo[42], M.X. Luo[80], T. Luo[12,f],

JHEP12(2023)072

X.L. Luo[1,58], X.R. Lyu[63], Y.F. Lyu[44], F.C. Ma[41], H.L. Ma[1], J.L. Ma[1,63], L.L. Ma[50], M.M. Ma[1,63], Q.M. Ma[1], R.Q. Ma[1,63], R.T. Ma[63], X.Y. Ma[1,58], Y. Ma[47,g], Y.M. Ma[32], F.E. Maas[19], M. Maggiora[74A,74C], S. Malde[69], A. Mangoni[29B], Y.J. Mao[47,g], Z.P. Mao[1], S. Marcello[74A,74C], Z.X. Meng[66], J.G. Messchendorp[14,64], G. Mezzadri[30A], H. Miao[1,63], T.J. Min[43], R.E. Mitchell[28], X.H. Mo[1,58,63], N.Yu. Muchnoi[13,b], Y. Nefedov[37], F. Nerling[19,d], I.B. Nikolaev[13,b], Z. Ning[1,58], S. Nisar[11,l], Y. Niu[50], S.L. Olsen[63], Q. Ouyang[1,58,63], S. Pacetti[29B,29C], X. Pan[55], Y. Pan[57], A. Pathak[35], P. Patteri[29A], Y.P. Pei[71,58], M. Pelizaeus[4], H.P. Peng[71,58], K. Peters[14,d], J.L. Ping[42], R.G. Ping[1,63], S. Plura[36], S. Pogodin[37], V. Prasad[34], F.Z. Qi[1], H. Qi[71,58], H.R. Qi[61], M. Qi[43], T.Y. Qi[12,f], S. Qian[1,58], W.B. Qian[63], C.F. Qiao[63], J.J. Qin[72], L.Q. Qin[15], X.P. Qin[12,f], X.S. Qin[50], Z.H. Qin[1,58], J.F. Qiu[1], S.Q. Qu[61], C.F. Redmer[36], K.J. Ren[40], A. Rivetti[74C], V. Rodin[64], M. Rolo[74C], G. Rong[1,63], Ch. Rosner[19], S.N. Ruan[44], N. Salone[45], A. Sarantsev[37,c], Y. Schelhaas[36], K. Schoenning[75], M. Scodeggio[30A,30B], K.Y. Shan[12,f], W. Shan[25], X.Y. Shan[71,58], J.F. Shangguan[55], L.G. Shao[1,63], M. Shao[71,58], C.P. Shen[12,f], H.F. Shen[1,63], W.H. Shen[63], X.Y. Shen[1,63], B.A. Shi[63], H.C. Shi[71,58], J.L. Shi[12], J.Y. Shi[1], Q.Q. Shi[55], R.S. Shi[1,63], X. Shi[1,58], J.J. Song[20], T.Z. Song[59], W.M. Song[35,1], Y.J. Song[12], Y.X. Song[47,g], S. Sosio[74A,74C], S. Spataro[74A,74C], F. Stieler[36], Y.J. Su[63], G.B. Sun[76], G.X. Sun[1], H. Sun[63], H.K. Sun[1], J.F. Sun[20], K. Sun[61], L. Sun[76], S.S. Sun[1,63], T. Sun[1,63], W.Y. Sun[35], Y. Sun[9], Y.J. Sun[71,58], Y.Z. Sun[1], Z.T. Sun[50], Y.X. Tan[71,58], C.J. Tang[54], G.Y. Tang[1], J. Tang[59], Y.A. Tang[76], L.Y. Tao[72], Q.T. Tao[26,h], M. Tat[69], J.X. Teng[71,58], V. Thoren[75], W.H. Tian[59], W.H. Tian[52], Y. Tian[32,63], Z.F. Tian[76], I. Uman[62B], S.J. Wang[50], B. Wang[1], B.L. Wang[63], Bo Wang[71,58], C.W. Wang[43], D.Y. Wang[47,g], F. Wang[72], H.J. Wang[39,j,k], H.P. Wang[1,63], J.P. Wang[50], K. Wang[1,58], L.L. Wang[1], M. Wang[50], Meng Wang[1,63], S. Wang[39,j,k], S. Wang[12,f], T. Wang[12,f], T.J. Wang[44], W. Wang[59], W. Wang[72], W.P. Wang[71,58], X. Wang[47,g], X.F. Wang[39,j,k], X.J. Wang[40], X.L. Wang[12,f], Y. Wang[61], Y.D. Wang[46], Y.F. Wang[1,58,63], Y.H. Wang[48], Y.N. Wang[46], Y.Q. Wang[1], Yaqian Wang[18,1], Yi Wang[61], Z. Wang[1,58], Z.L. Wang[72], Z.Y. Wang[1,63], Ziyi Wang[63], D. Wei[70], D.H. Wei[15], F. Weidner[68], S.P. Wen[1], C.W. Wenzel[4], U.W. Wiedner[4], G. Wilkinson[69], M. Wolke[75], L. Wollenberg[4], C. Wu[40], J.F. Wu[1,63], L.H. Wu[1], L.J. Wu[1,63], X. Wu[12,f], X.H. Wu[35], Y. Wu[71], Y.J. Wu[32], Z. Wu[1,58], L. Xia[71,58], X.M. Xian[40], T. Xiang[47,g], D. Xiao[39,j,k], G.Y. Xiao[43], H. Xiao[12,f], S.Y. Xiao[1], Y.L. Xiao[12,f], Z.J. Xiao[42], C. Xie[43], X.H. Xie[47,g], Y. Xie[50], Y.G. Xie[1,58], Y.H. Xie[6], Z.P. Xie[71,58], T.Y. Xing[1,63], C.F. Xu[1,63], C.J. Xu[59], G.F. Xu[1], H.Y. Xu[66], Q.J. Xu[17], Q.N. Xu[31], W. Xu[1,63], W.L. Xu[66], X.P. Xu[55], Y.C. Xu[78], Z.P. Xu[43], Z.S. Xu[63], F. Yan[12,f], L. Yan[12,f], W.B. Yan[71,58], W.C. Yan[81], X.Q. Yan[1], H.J. Yang[51,e], H.L. Yang[35], H.X. Yang[1], Tao Yang[1], Y. Yang[12,f], Y.F. Yang[44], Y.X. Yang[1,63], Yifan Yang[1,63], Z.W. Yang[39,j,k], Z.P. Yao[50], M. Ye[1,58], M.H. Ye[8], J.H. Yin[1], Z.Y. You[59], B.X. Yu[1,58,63], C.X. Yu[44], G. Yu[1,63], J.S. Yu[26,h], T. Yu[72], X.D. Yu[47,g], C.Z. Yuan[1,63], L. Yuan[2], S.C. Yuan[1], X.Q. Yuan[1], Y. Yuan[1,63], Z.Y. Yuan[59], C.X. Yue[40], A.A. Zafar[73], F.R. Zeng[50], X. Zeng[12,f], Y. Zeng[26,h], Y.J. Zeng[1,63], X.Y. Zhai[35], Y.C. Zhai[50], Y.H. Zhan[59], A.Q. Zhang[1,63], B.L. Zhang[1,63], B.X. Zhang[1], D.H. Zhang[44], G.Y. Zhang[20], H. Zhang[71], H.H. Zhang[59], H.H. Zhang[35], H.Q. Zhang[1,58,63], H.Y. Zhang[1,58], J.J. Zhang[52], J.L. Zhang[21], J.Q. Zhang[42], J.W. Zhang[1,58,63], J.X. Zhang[39,j,k], J.Y. Zhang[1], J.Z. Zhang[1,63], Jianyu Zhang[63], Jiawei Zhang[1,63], L.M. Zhang[61], L.Q. Zhang[59], Lei Zhang[43], P. Zhang[1], Q.Y. Zhang[40,81], Shuihan Zhang[1,63], Shulei Zhang[26,h,m], X.D. Zhang[46], X.M. Zhang[1], X.Y. Zhang[50], X.Y. Zhang[55], Y. Zhang[69], Y. Zhang[72], Y.T. Zhang[81], Y.H. Zhang[1,58], Yan Zhang[71,58], Yao Zhang[1],

JHEP12(2023)072

Z.H. Zhang[1], Z.L. Zhang[35], Z.Y. Zhang[44], Z.Y. Zhang[76], G. Zhao[1], J. Zhao[40], J.Y. Zhao[1,63], J.Z. Zhao[1,58], Lei Zhao[71,58], Ling Zhao[1], M.G. Zhao[44], S.J. Zhao[81], Y.B. Zhao[1,58], Y.X. Zhao[32,63], Z.G. Zhao[71,58], A. Zhemchugov[37,a], B. Zheng[72], J.P. Zheng[1,58], W.J. Zheng[1,63], Y.H. Zheng[63], B. Zhong[42], X. Zhong[59], H. Zhou[50], L.P. Zhou[1,63], X. Zhou[76], X.K. Zhou[6], X.R. Zhou[71,58], X.Y. Zhou[40], Y.Z. Zhou[12,f], J. Zhu[44], K. Zhu[1], K.J. Zhu[1,58,63], L. Zhu[35], L.X. Zhu[63], S.H. Zhu[70], S.Q. Zhu[43], T.J. Zhu[12,f], W.J. Zhu[12,f], Y.C. Zhu[71,58], Z.A. Zhu[1,63], J.H. Zou[1], J. Zu[71,58]

[1] *Institute of High Energy Physics, Beijing 100049, People's Republic of China*
[2] *Beihang University, Beijing 100191, People's Republic of China*
[3] *Beijing Institute of Petrochemical Technology, Beijing 102617, People's Republic of China*
[4] *Bochum Ruhr-University, D-44780 Bochum, Germany*
[5] *Carnegie Mellon University, Pittsburgh, Pennsylvania 15213, USA*
[6] *Central China Normal University, Wuhan 430079, People's Republic of China*
[7] *Central South University, Changsha 410083, People's Republic of China*
[8] *China Center of Advanced Science and Technology, Beijing 100190, People's Republic of China*
[9] *China University of Geosciences, Wuhan 430074, People's Republic of China*
[10] *Chung-Ang University, Seoul, 06974, Republic of Korea*
[11] *COMSATS University Islamabad, Lahore Campus, Defence Road, Off Raiwind Road, 54000 Lahore, Pakistan*
[12] *Fudan University, Shanghai 200433, People's Republic of China*
[13] *G.I. Budker Institute of Nuclear Physics SB RAS (BINP), Novosibirsk 630090, Russia*
[14] *GSI Helmholtzcentre for Heavy Ion Research GmbH, D-64291 Darmstadt, Germany*
[15] *Guangxi Normal University, Guilin 541004, People's Republic of China*
[16] *Guangxi University, Nanning 530004, People's Republic of China*
[17] *Hangzhou Normal University, Hangzhou 310036, People's Republic of China*
[18] *Hebei University, Baoding 071002, People's Republic of China*
[19] *Helmholtz Institute Mainz, Staudinger Weg 18, D-55099 Mainz, Germany*
[20] *Henan Normal University, Xinxiang 453007, People's Republic of China*
[21] *Henan University, Kaifeng 475004, People's Republic of China*
[22] *Henan University of Science and Technology, Luoyang 471003, People's Republic of China*
[23] *Henan University of Technology, Zhengzhou 450001, People's Republic of China*
[24] *Huangshan College, Huangshan 245000, People's Republic of China*
[25] *Hunan Normal University, Changsha 410081, People's Republic of China*
[26] *Hunan University, Changsha 410082, People's Republic of China*
[27] *Indian Institute of Technology Madras, Chennai 600036, India*
[28] *Indiana University, Bloomington, Indiana 47405, USA*
[29] *INFN Laboratori Nazionali di Frascati, (A)INFN Laboratori Nazionali di Frascati, I-00044, Frascati, Italy; (B)INFN Sezione di Perugia, I-06100, Perugia, Italy; (C)University of Perugia, I-06100, Perugia, Italy*
[30] *INFN Sezione di Ferrara, (A)INFN Sezione di Ferrara, I-44122, Ferrara, Italy; (B)University of Ferrara, I-44122, Ferrara, Italy*
[31] *Inner Mongolia University, Hohhot 010021, People's Republic of China*
[32] *Institute of Modern Physics, Lanzhou 730000, People's Republic of China*
[33] *Institute of Physics and Technology, Peace Avenue 54B, Ulaanbaatar 13330, Mongolia*
[34] *Instituto de Alta Investigación, Universidad de Tarapacá, Casilla 7D, Arica, Chile*
[35] *Jilin University, Changchun 130012, People's Republic of China*
[36] *Johannes Gutenberg University of Mainz, Johann-Joachim-Becher-Weg 45, D-55099 Mainz, Germany*
[37] *Joint Institute for Nuclear Research, 141980 Dubna, Moscow region, Russia*
[38] *Justus-Liebig-Universitaet Giessen, II. Physikalisches Institut, Heinrich-Buff-Ring 16, D-35392 Giessen, Germany*
[39] *Lanzhou University, Lanzhou 730000, People's Republic of China*
[40] *Liaoning Normal University, Dalian 116029, People's Republic of China*

JHEP12(2023)072

[41] Liaoning University, Shenyang 110036, People's Republic of China
[42] Nanjing Normal University, Nanjing 210023, People's Republic of China
[43] Nanjing University, Nanjing 210093, People's Republic of China
[44] Nankai University, Tianjin 300071, People's Republic of China
[45] National Centre for Nuclear Research, Warsaw 02-093, Poland
[46] North China Electric Power University, Beijing 102206, People's Republic of China
[47] Peking University, Beijing 100871, People's Republic of China
[48] Qufu Normal University, Qufu 273165, People's Republic of China
[49] Shandong Normal University, Jinan 250014, People's Republic of China
[50] Shandong University, Jinan 250100, People's Republic of China
[51] Shanghai Jiao Tong University, Shanghai 200240, People's Republic of China
[52] Shanxi Normal University, Linfen 041004, People's Republic of China
[53] Shanxi University, Taiyuan 030006, People's Republic of China
[54] Sichuan University, Chengdu 610064, People's Republic of China
[55] Soochow University, Suzhou 215006, People's Republic of China
[56] South China Normal University, Guangzhou 510006, People's Republic of China
[57] Southeast University, Nanjing 211100, People's Republic of China
[58] State Key Laboratory of Particle Detection and Electronics, Beijing 100049, Hefei 230026, People's Republic of China
[59] Sun Yat-Sen University, Guangzhou 510275, People's Republic of China
[60] Suranaree University of Technology, University Avenue 111, Nakhon Ratchasima 30000, Thailand
[61] Tsinghua University, Beijing 100084, People's Republic of China
[62] Turkish Accelerator Center Particle Factory Group, (A)Istinye University, 34010, Istanbul, Turkey; (B)Near East University, Nicosia, North Cyprus, 99138, Mersin 10, Turkey
[63] University of Chinese Academy of Sciences, Beijing 100049, People's Republic of China
[64] University of Groningen, NL-9747 AA Groningen, The Netherlands
[65] University of Hawaii, Honolulu, Hawaii 96822, USA
[66] University of Jinan, Jinan 250022, People's Republic of China
[67] University of Manchester, Oxford Road, Manchester, M13 9PL, United Kingdom
[68] University of Muenster, Wilhelm-Klemm-Strasse 9, 48149 Muenster, Germany
[69] University of Oxford, Keble Road, Oxford OX13RH, United Kingdom
[70] University of Science and Technology Liaoning, Anshan 114051, People's Republic of China
[71] University of Science and Technology of China, Hefei 230026, People's Republic of China
[72] University of South China, Hengyang 421001, People's Republic of China
[73] University of the Punjab, Lahore-54590, Pakistan
[74] University of Turin and INFN, (A)University of Turin, I-10125, Turin, Italy; (B)University of Eastern Piedmont, I-15121, Alessandria, Italy; (C)INFN, I-10125, Turin, Italy
[75] Uppsala University, Box 516, SE-75120 Uppsala, Sweden
[76] Wuhan University, Wuhan 430072, People's Republic of China
[77] Xinyang Normal University, Xinyang 464000, People's Republic of China
[78] Yantai University, Yantai 264005, People's Republic of China
[79] Yunnan University, Kunming 650500, People's Republic of China
[80] Zhejiang University, Hangzhou 310027, People's Republic of China
[81] Zhengzhou University, Zhengzhou 450001, People's Republic of China

[a] Also at the Moscow Institute of Physics and Technology, Moscow 141700, Russia
[b] Also at the Novosibirsk State University, Novosibirsk, 630090, Russia
[c] Also at the NRC "Kurchatov Institute", PNPI, 188300, Gatchina, Russia
[d] Also at Goethe University Frankfurt, 60323 Frankfurt am Main, Germany
[e] Also at Key Laboratory for Particle Physics, Astrophysics and Cosmology, Ministry of Education; Shanghai Key Laboratory for Particle Physics and Cosmology; Institute of Nuclear and Particle Physics, Shanghai 200240, People's Republic of China

JHEP12(2023)072

[f] Also at Key Laboratory of Nuclear Physics and Ion-beam Application (MOE) and Institute of Modern Physics, Fudan University, Shanghai 200443, People's Republic of China
[g] Also at State Key Laboratory of Nuclear Physics and Technology, Peking University, Beijing 100871, People's Republic of China
[h] Also at School of Physics and Electronics, Hunan University, Changsha 410082, China
[i] Also at Guangdong Provincial Key Laboratory of Nuclear Science, Institute of Quantum Matter, South China Normal University, Guangzhou 510006, China
[j] Also at Frontiers Science Center for Rare Isotopes, Lanzhou University, Lanzhou 730000, People's Republic of China
[k] Also at Lanzhou Center for Theoretical Physics, Lanzhou University, Lanzhou 730000, People's Republic of China
[l] Also at the Department of Mathematical Sciences, IBA, Karachi 75270, Pakistan
[m] Also at Greater Bay Area Institute for Innovation, Hunan University, Guangzhou 511300, Guangdong Province, China

JHEP12(2023)072